PHYSICAL REVIEW B VOLUME 4, NUMBER 2 15 JULY 1971

# Thermal Conductivity of Garnets and Phonon Scattering by Rare-Earth Ions*

Glen A. Slack and D. W. Oliver
*General Electric Research & Development Center, Schenectady, New York* 12301

(Received 12 March 1971)

The thermal conductivity of 23 different single crystals of natural and synthetic garnets has been measured from 2 to 300 K. The heat is carried by phonons. Because the garnets have 80 atoms per primitive unit cell, there are a large number of optical-phonon modes which apparently do not contribute to the heat transport. The heat seems to be carried mainly by the acoustic phonons with wave numbers less than about 125 $\mathrm{cm}^{-1}$. These acoustic phonons can be scattered by rare-earth ions that have electronic levels of their partially filled 4f shells that are at energies of 125 $\mathrm{cm}^{-1}$ or less above the ground state. Such phonon scattering has been observed in the aluminum and gallium garnets of the trivalent ions Dy, Tb, Tm, Er, and Ho. The strength of the phonon scattering decreases in the order listed. This "magnetic scattering" is absent for trivalent Y, Gd, and Lu.

## I. INTRODUCTION

The thermal conductivity $\kappa$ of a number of different single-crystal garnets has been studied over the temperature range 2–300 K. The purpose of this study is to determine the intrinsic phonon thermal conductivity of the rather complex garnet lattice, and to determine whether the phonon scattering from various trivalent rare-earth ions substituted into this lattice is observable. Previous studies of the $\kappa$ of garnet crystals have been made on $Y_3Fe_5O_{12}$,[1–5] $Y_3Al_5O_{12}$,[4,6] $Y_3Ga_5O_{12}$,[7] and $Dy_3Al_5O_{12}$.[8] Theoretical calculations have also been made for $Y_3Fe_5O_{12}$.[9,10] The studies[1–7] show that the crystals have a $\kappa$ of about 0.07 to 0.10 W/cm K at 300 K and reach a $\kappa$ maximum of 1–5 W/cmK near 20 K. There is some suggestion[1–3,5,9,10] of a magnon heat transport in $Y_3Fe_5O_{12}$ and also[8] in $Dy_3Al_5O_{12}$ for temperatures below 4 K. There are no $\kappa$ measurements on $Y_3Fe_5O_{12}$ crystals through the region of its Curie temperature at 560 K. Some ceramic samples[11] of $Y_3Fe_5O_{12}$-$Ca_3Fe_2Si_3O_{12}$ have shown anomalies in $\kappa$ near their Curie temperatures. There are no reports of resonant scattering of phonons[12,13] from the low-lying electronic levels[14] of the rare-earth ions in garnets. Phonon scattering has been seen from Ho in holmium ethyl sulfate[15,16]; Ce, Dy, Ho, and Yb in crystals[17,18] of $CaF_2$; and from Nd in crystals[4,6,19] of $CaWO_4$, $Y_3Al_5O_{12}$, and $Y_2O_3$. Some other thermal conductivity studies[20–22] on semiconducting compounds containing rare-earth ions may show signs of phonon scattering by the rare-earth ions, but this interpretation is questionable at present.

Of great importance to the present study are the electronic energy levels of the ground-state manifold of the trivalent rare-earth ions in the dodecahedral sites of the garnet lattice. Many of the levels have been determined by optical techniques for Nd,[23–26] Gd,[27] Tb,[28–33] Dy,[34–39] Ho,[40–47] Er,[48–50] Tm,[40,51–55] and Yb.[56] The energies of these levels, except for Nd, are given in Table I. Since an energy of 1 $\mathrm{cm}^{-1}$ corresponds to $kT$ with $T = 1.44$ K, it can be seen from Table I that many ions have levels in the temperature range of 2–300 K that we are studying. Thus if the rare-earth ions exhibit a phonon scattering due to phonon-induced transitions of electrons between these various levels, we might see it by studying $\kappa$ over this temperature range.

## II. SAMPLES

### A. Natural Garnets

We have studied a large number of single-crystal samples of natural and synthetic garnets. The natural crystals are listed in Table II. The divalent ion composition was determined by standard chemical techniques. The divalent ions occur mainly in the dodecahedral or $R$ sites in $R_3Al_2Si_3O_{12}$ garnet. Table II shows the fraction of the $R$ sites occupied by $Fe^{2+}$ or $Mn^{2+}$ ions. Optical-absorption studies on these same crystals have been reported,[57] and show the absorption bands of the $Fe^{2+}$ and the $Mn^{2+}$, as well as other impurities present. The spessartite, rhodolite, and alamandite are essentially $(Mg, Fe, Mn)_3Al_2Si_3O_{12}$ while the hessonite and grossularite are essentially $Ca_3Al_2Si_3O_{12}$. The complete analyses are given in Ref. 57.

### B. Synthetic Garnets

A number of single crystals of synthetic garnet were studied, as shown in Table III. They were grown either by use of PbO-$PbF_2$ flux techniques or were pulled from the melt. The samples used for the $\kappa$ measurements were in the shape of rods with a square or a nearly square rectangular cross section. The sample length and average diameter are given in Table III. Since $\kappa$ is sensitive to impurities in the crystals, the impurity contents are given in Table IV. The flux-grown crystals all contained rather large amounts of impurity, and the impurity range found is shown. The melt-grown crystals were considerably purer, and several analyses are given. The purest crystal, $Y_3Al_5O_{12}$-*R*186, was analyzed by using a mass spectrometer. The residual impurities found were only those in the $Y_2O_3$ starting material as supplied by the manufacturer.[58] The $Al_2O_3$ starting material was much purer.[59] The optical-absorption spectrum of *R*186 has been published[60] (see sample *M*28 of Ref. 60). The optical-absorption curve shows very little impurity absorption.

One check on the identity and the stoichiometry of the garnet crystals is furnished by the x-ray lattice parameter. This measurement is particularly useful when samples are collected from a number of different sources, as shown in Table II. The results are plotted in Fig. 1. There is generally a smooth variation in $a_0$ with the atomic number of the rare-earth ion. Similar plots have been given by Bertaut and Forrat,[61] Euler and Bruce,[62] and Rubenstein and Barns.[63] Further data on lattice parameters and their variation with stoichiometry are given by Schneider *et al.*[64] The points for $Lu_3Al_5O_{12}$ and $Lu_3Ga_5O_{12}$ plotted as open circles in Fig. 1 are from these latter three sources. Schneider *et al.*[64] point out that the stoichiometry of garnets can vary in the direction of excess rare-earth ions. In the Al garnets this appears to happen for only Yb and Lu garnets. The dashed curve in Fig. 1 shows the approximate upper limits to the lattice parameters. For $Lu_2Al_5O_{12}$ this corresponds to about 1 mole% excess $Lu_2O_3$. The data point for sample *R*177 of $Lu_3Al_5O_{12}$ at $a_0 = 11.9171$ Å lies above the curve and indicates about 0.3 mole% excess of $Lu_2O_3$ in the crystal, i.e., 37.8 mole% $Lu_2O_3$ instead of 37.5 mole%, the stoichiometric composition. Similarly, the sample *R*160 of $Tb_3Ga_5O_{12}$ with $a_0 = 12.3476$ Å appears to contain 0.5 mole% excess $Tb_2O_3$. Schneider *et al.*[64] estimate that the maximum excess in this garnet is about 6 mole%. Hence these melt-grown crystals are stoichiometric to within 0.5 mole%.

## III. EXPERIMENTAL TECHNIQUE

The x-ray lattice constants of the various garnets were determined from a Debye-Scherrer powder pattern taken on a General Electric XRD-4 apparatus using Cu *Kα* radiation. A computerized least-squares analysis gives $a_0$ to ± 0.0005 Å. The thermal conductivity vs temperature curves of the

TABLE I. Energy levels of the ground-state multiplet of trivalent rare-earth ions in garnets.

| Ion | Host crystal | Multiplet | Number of levels | Wave numbers of observed levels (cm$^{-1}$)[a] | Reference |
|---|---|---|---|---|---|
| $Gd^{3+}$ | GdAl*G*[b] | $^8S_0$ | 1 | 0 | 27 |
| $Gd^{3+}$ | GdGa*G* | $^8S_0$ | 1 | 0 | 27 |
| $Tb^{3+}$ | TbAl*G* | $^7F_6$ | 13 | 0, 4, 61, 75, 86, 137, 145, 180, 234, 263, 292, 357, 367 | 28–31 |
| $Tb^{3+}$ | YAl*G* | $^7F_6$ | 13 | 0, 5, 61, 70, 82, 116, 207, 270, 432, 443 | 29, 32 |
| $Tb^{3+}$ | TbGa*G* | $^7F_6$ | 13 | unknown | ... |
| $Tb^{3+}$ | YGa*G* | $^7F_6$ | 13 | unknown | ... |
| $Tb^{3+}$ | YFe*G* | $^7F_6$ | 13 | 0, 6, 38, 40, 50, 55 | 33 |
| $Dy^{3+}$ | DyAl*G* | $^6H_{15/2}$ | 8 | 0, 70, 116, 197, 256 | 34–36 |
| $Dy^{3+}$ | YAl*G* | $^6H_{15/2}$ | 8 | 0, 61, 101, 175, 234, (474), (517), 741 | 34, 37, 38 |
| $Dy^{3+}$ | DyGa*G* | $^6H_{15/2}$ | 8 | 0, 22, 71 | 36, 37, 39 |
| $Dy^{3+}$ | YGa*G* | $^6H_{15/2}$ | 8 | 0, 20, 71, 118, 149, (466), (508), 579 | 37, 38 |
| $Ho^{3+}$ | HoAl*G* | $^5I_8$ | 17 | 0, 36, 42, 54, 63 | 40 |
| $Ho^{3+}$ | YAl*G* | $^5I_8$ | 17 | 0, 39, 50, 138, 156, 416, 437, 444, 462, 494, 518, 532 | 41 |
| $Ho^{3+}$ | HoGa*G* | $^5I_8$ | 17 | 0, 6, 27, 30, 39, 44 | 42–44 |
| $Ho^{3+}$ | YGa*G* | $^5I_8$ | 17 | 0, 5, 8, 30, 43, 94, 111, 113, 380, 418, 428, 432, 447, 481 | 45–47 |
| $Er^{3+}$ | ErAl*G* | $^4I_{15/2}$ | 8 | 0, 27, 58, 79, 423, 436, 530, 574 | 48 |
| $Er^{3+}$ | ErGa*G* | $^4I_{15/2}$ | 8 | 0, 46, 55, 76 | 49 |
| $Er^{3+}$ | YGa*G* | $^4I_{15/2}$ | 8 | 0, 44, 49, 76, 422, 430, 490, 527 | 50 |
| $Tm^{3+}$ | TmAl*G* | $^3H_6$ | 13 | 0, 35 | 40, 51 |
| $Tm^{3+}$ | Yal*G* | $^3H_6$ | 13 | 0, 28, 43, 228, 240, 270, 490, 582 | 52–54 |
| $Tm^{3+}$ | TmGa*G* | $^3H_6$ | 13 | 0, 63, 85, 113, 123, 184 | 51, 54 |
| $Tm^{3+}$ | YGa*G* | $^3H_6$ | 13 | 0, 64, 87, 99, 188 | 54, 55 |
| $Yb^{3+}$ | YbAl*G* | $^2F_{7/2}$ | 4 | 0, 618, 701, 766 | 56 |
|  | YbGa*G* | $^2F_{7/2}$ | 4 | 0, 546, 599, 624 | 56 |

[a] The level energies enclosed in parentheses are theoretical estimates.

[b] The final *G* here and in the other crystals listed stands for garnet.

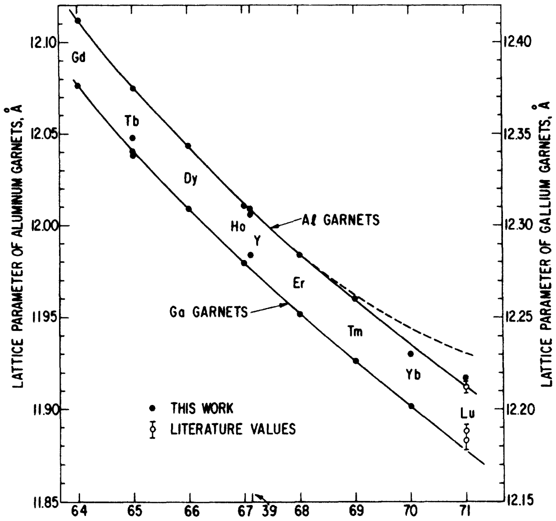

FIG. 1. Lattice parameters of rare-earth aluminum and gallium garnets as a function of the atomic number of the rare-earth ion. The solid lines indicate the curves for stoichiometric garnets. The dashed line for the aluminum garnets indicates the approximate upper limits for crystals containing excess rare-earth ions. The upper limits for nonstoichiometric gallium garnets are much greater.

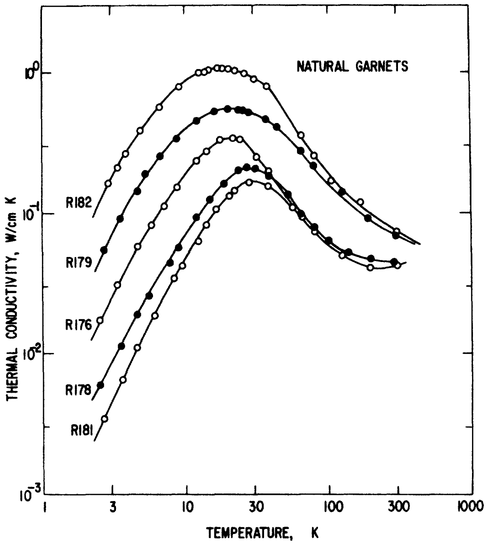

FIG. 2. Thermal conductivity vs temperature for five different natural garnet crystals.

crystals were measured in an apparatus[65] that has been described previously. The temperature dependence of $\kappa$ is accurate to ±5% while the absolute value of $\kappa$ depends on the sample length. $\kappa$ is conservatively estimated to be accurate to ±10%.

## IV. EXPERIMENTAL RESULTS

The $\kappa$ vs $T$ curves for the five natural garnet crystals are given in Fig. 2. The numbers $R$182, etc., identify the experimental run in which the thermal conductivity was measured. The $R$ numbers run chronologically based on the data at which the measurements were actually made.[65–67] From Table II it can be seen that $R$182 is the crystal with the smallest transition-metal concentration and $R$178 has the largest. The $\kappa$ appears to decrease as the Fe plus Mn concentration increases. Thus we choose $R$182 as the sample with the least amount of impurity scattering of phonons. Hence its $\kappa$ vs $T$ curve for $T > 40$ K ought to be nearly equal to that of a pure $Ca_3Al_2Si_3O_4$ natural garnet. Values of $\kappa$ vs $T$ as read from Fig. 2 are given in Table V for $T > 40$ K. For $T < 40$ K the results depend on the sample geometry, and are not an intrinsic property.

The $Ca_3Al_2Si_3O_4$ results should be comparable to those for other synthetic garnets that have no magnetic ions such as $Y_3Al_5O_{12}$, $Lu_3Al_5O_{12}$, and $Y_3Ga_5O_{12}$. The $\kappa$ results for $Y_3Al_5O_{12}$ are given in Figs. 3–5; the curve for $Lu_3Al_5O_{12}$ is in Fig. 6; the curve for $Y_3Ga_5O_{12}$ is in Fig. 7. The intrinsic $\kappa$ vs $T$ values for these crystals in the temperature region where $\kappa$ is not dependent on the sample size are given in Tables VI and VII. Note that, indeed, the $\kappa$ values for these crystals are close to those for $Ca_3Al_2Si_3O_{12}$.

For those crystals which have rare-earth ions that bear a magnetic moment, i.e., have a partially filled $4f$ shell, we distinguish between the ions that

TABLE II. Properties of the natural garnet crystals.

| Crystal | Run No. | Lattice constant (Å) | Crystal size $l$ (mm) | $d$ (mm) | Impurity concentration[a] $Fe^{2+}$ | $Mn^{2+}$ |
|---|---|---|---|---|---|---|
| Spessartite | $R$176 | 11.554 | 6.1 | 2.7 | 0.02 | 0.21 |
| Rhodolite | $R$178 | 11.509 | 8.6 | 2.9 | 0.56 | ••• |
| Almandite | $R$181 | 11.512 | 11.1 | 3.1 | 0.49 | 0.02 |
| Hessonite | $R$179 | 11.854 | 5.5 | 2.5 | 0.07 | ••• |
| Grossularite | $R$182 | 11.846 | 5.7 | 2.8 | 0.03 | 0.01 |

[a] The five crystals varied mainly with respect to the divalent ion composition $R$ in the formula $R_3Al_2Si_3O_{12}$. The Fe and Mn concentrations are the fractions of the $R$ sites occupied by $Fe^{2+}$ or $Mn^{2+}$.

have electronic energy levels in the ground-state manifold that lie within the energy range $kT$, where $2 \le T \le 300$ K, and those that only have levels higher than 300 K. From Table I all the ions except $Gd^{3+}$ and $Yb^{3+}$ have levels in this lower-energy range. Thus we expect the Gd and Ub garnets to have $\kappa$ vs $T$ curves similar to those of the nonmagnetic garnets. This is borne out by the experimental results for $Gd_3Al_5O_{12}$ in Fig. 5, $Yb_3Al_5O_{12}$ in Fig. 6, and $Gd_3Ga_5O_{12}$ and $Yb_3Ga_5O_{12}$ in Figs. 7 and 8. The $\kappa$ vs $T$ curves for the Al and Ga garnets of Tb, Dy, Ho, Er, and Tm in Figs. 5, 6, 8–10 show $\kappa$ values that are reduced below those of the other garnets because of an increased scattering of the phonons.

In Fig. 11 we show the $\kappa$ vs $T$ results for four samples of $Y_3Fe_5O_{12}$. In the range above 30 K the results look like those for the Ga garnets in Fig. 7. In the temperature range below 10 K there is some source of phonon scattering which is probably associated with chemical impurities in the lattices.

In order to investigate the low-temperature region below 30 K, where the $\kappa$ value depends on the sample geometry, we have taken sample *R*186 of $Y_3Al_5O_{12}$ and have measured $\kappa$ as a function of diameter. The results at the smallest diameter are shown as *R*195 in Fig. 3. The value of $\kappa$ below 30 K is dependent on the sample diameter $d$. Actually three different diameters were used: 2.95, 1.53, and 0.81 mm. The results for the 1.53-mm crystal *R*194 lie between those for *R*186 and *R*195 in Fig. 3, but the $\kappa$ vs $T$ curve is not shown. The values of $\kappa$ (at 3 K) vs $d$ for this series are shown in Fig. 4. The surfaces of the crystal were finely ground to look like ground glass in all cases, and the long dimension of the crystal rod was a [100] axis. Note that $\kappa$ is proportional to $d$ in Fig. 4.

TABLE III. Synthetic garnet crystals studied.

| Crystal | Run No. | $a_0$[a] Å ±0.0005 | Crystal size (mm) | | Source | Growth |
|---|---|---|---|---|---|---|
| | | | $l$[b] | $d$[c] | | |
| YAl*G* | *R*142 | 12.0093 | 18.9 | 3.5 | UC[d] | melt[e] |
| YAl*G* | *R*186 | 12.0090 | 10.0 | 3.0 | GE[f] | melt |
| YAl*G* | *R*193 | 12.0063 | 6.0 | 3.0 | Airtron[g] | flux[h] |
| YAl*G* | *R*195 | 12.0090 | 10.0 | 0.8 | *R*186 | cut down |
| GdAl*G* | *R*199 | 12.1116 | 3.8 | 2.2 | Airtron | flux |
| TbAl*G* | *R*148 | 12.0737 | 3.3 | 1.8 | CBR[i] | flux |
| TbAl*G* | *R*154 | 12.0749 | 3.6 | 2.0 | Yale[j] | flux |
| DyAl*G* | *R*161 | 12.0431 | 6.7 | 2.2 | Yale | flux |
| DyAl*G* | *R*185 | 12.0441 | 9.8 | 2.9 | UC | melt |
| HoAl*G* | *R*203 | 12.0107 | 3.7 | 2.0 | Airtron | flux |
| ErAl*G* | *R*168 | 11.9839 | 5.2 | 1.4 | Yale | flux |
| TmAl*G* | *R*172 | 11.9601 | 7.2 | 2.0 | GE | melt |
| YbAl*G* | *R*204 | 11.9300 | 3.2 | 2.0 | Airtron | flux |
| LuAl*G* | *R*177 | 11.9171 | 7.2 | 2.3 | GE | melt |
| LuAl*G* | *R*197 | 11.9178 | 8.4 | 1.8 | GE | melt |
| YGa*G* | *R*155 | 12.2837 | 4.7 | 1.7 | Yale | flux |
| GdGa*G* | *R*157 | 12.3763 | 5.9 | 1.8 | Yale | flux |
| TbGa*G* | *R*156 | 12.3403 | 2.8 | 2.1 | Yale | flux |
| TbGa*G* | *R*160 | 12.3476 | 7.6 | 3.1 | GE | melt |
| TbGa*G* | *R*165 | 12.3383 | 5.0 | 2.6 | Yale | flux |
| DyGa*G* | *R*200 | 12.3087 | 5.5 | 1.8 | Airtron | flux |
| HoGa*G* | *R*158 | 12.2796 | 2.6 | 1.7 | Yale | flux |
| ErGa*G* | *R*170 | 12.2516 | 6.9 | 1.8 | Yale | flux |
| TmGa*G* | *R*159 | 12.2262 | 3.8 | 1.9 | Yale | flux |
| YbGa*G* | *R*173 | 12.2014 | 4.7 | 2.1 | Yale | flux |
| YFe*G* | *R*136 | 12.3766 | 11.3 | 3.9 | Airtron | flux |
| YFe*G* | *R*166 | 12.38 | 13.0 | 4.2 | Airtron | flux |
| YFe*G* | *R*175 | 12.38 | 24.8 | 3.1 | Airtron | flux |
| YFe*G* | *R*205 | 12.3766 | 11.3 | 1.2 | *R*136 | cut down |

[a] Lattice constant of crystal.

[b] Sample length used for determining the thermal conductivity.

[c] Average diameter used for determing the thermal conductivity.

[d] Union Carbide Corp., Boston, Mass.

[e] Pulled from the melt, Czochralski method.

[f] General Electric Research and Development Center, Schenectady, N. Y.

[g] Airtron, Morris Plains, N. J.

[h] Grown from a PbO-$PbF_2$ flux.

[i] Charles B. Rubinstein, Bell Telephone Labs, Murray Hill, N. J.

[j] Yale University, New Haven, Conn. Samples supplied by courtesy of Professor Werner P. Wolf.

TABLE IV. Impurity concentrations in various synthetic garnets.

| Crystal | Impurity | Concentration in ppm by weight |
|---|---|---|
| Typical flux-grown garnet | B | 0–100 |
| | Cu | 0–30 |
| | Fe | 30–300 |
| | Mg | 0–100 |
| | Pb | 100–2000 |
| | Pt | 0–300 |
| | Si | 30–1000 |
| | Ti | 0–30 |
| | Rare earths[a] | 50–500 |
| YAl*G*-*R*186[b] melt grown | Ca | 7 |
| | Ir | $\leq 2$ |
| | Mg | 10 |
| | Fe | 7 |
| | Si | 15 |
| | Rare earths | < 1 |
| YAl*G*-*R*193 flux grown | Ca | 700 |
| | Mg | < 10 |
| | Fe | 20 |
| | Pb | 30 |
| | Si | 10 |
| | Rare earths | < 500 |
| TbGa*G*-*R*160 melt grown | Ca, Mg, Fe, Si | each < 10 |
| DyAl*G*-*R*185 melt grown | Ca | 10–100 |
| | Cu, Mg, Fe | each 1–10 |
| | Si | 3–30 |
| | La | 100–500 |
| | Rare earths | 10–100 |
| TmAl*G*-*R*172 melt grown | Fe | < 10 |
| LuAl*G*-*R*177[b] melt grown[c] | Fe | 1 |
| | Si | 30 |
| | Ce | 100 |
| | Y | 3 |
| | Rare earths | < 3 |
| YFe*G*-*R*136 flux | Al | 20 |
| | Mn | 50 |
| | Na | ~ 1000 |
| | Pb | < 10 |
| | Si | 30 |
| YFe*G*-*R*166[d] flux grown | Al | 50 |
| | Mn | 30 |
| | Na | < 500 |
| | Pb | ~ 1000 |
| | Si | 50 |

[a] Indicates those rare-earth elements that are nearby in the Periodic Table. For Y this means Ho and the adjacent elements.

[b] These were determined with a mass spectrometer; the other crystals were studied with an emission spectrograph.

[c] The Ce contamination was in the $Lu_2O_3$ from American Potash Corp. (Ref. 58). Sample *R*197 is similar to *R*177 except that the Ce concentration is about 10 ppm.

[d] The ferromagnetic resonance linewidth at 300 K was 1 Oe.

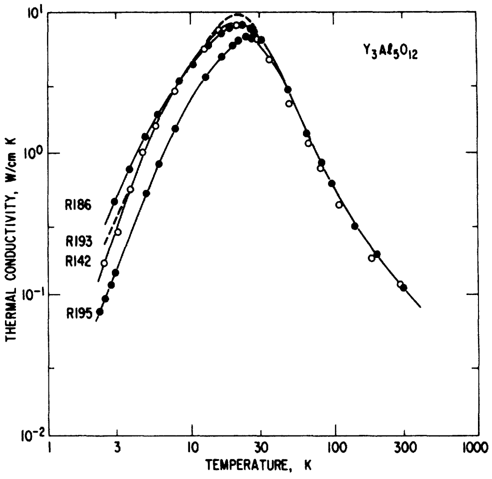

FIG. 3. Thermal conductivity vs temperature for three different $Y_3Al_5O_{12}$ crystals. Sample *R*195 is just sample *R*186 reduced in diameter.

The same type of experiment was performed on sample *R*136 of $Y_3Fe_5O_{12}$ which was a [100] axis rod (see Fig. 11). In this case the reduction of *d* by a factor of 0.4 (see *R*205), resulted in a reduction of $\kappa$ at 3 K by only a factor of 0.76. In this case $\kappa$ is not proportional to *d*.

Crystals of $Dy_3Al_5O_{12}$ are known[68–72] to undergo a magnetic transition at the antiferromagnetic Néel temperature of 2.54 K. We have carefully measured $\kappa$ vs *T* through this temperature range on sample *R*161. The results are shown in Fig. 12. There is no obvious anomaly in the $\kappa$ curve at

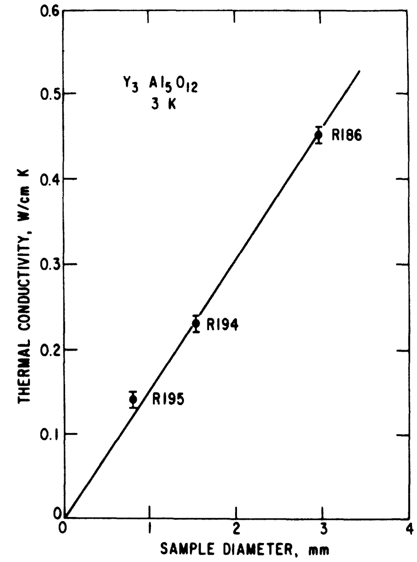

FIG. 4. Thermal conductivity at 3 K of sample *R*186 of $Y_3Al_5O_{12}$ for three different diameters (see Fig. 3). The complete curve for *R*194 is not given. The long dimension of the sample was the [100] crystal axis.

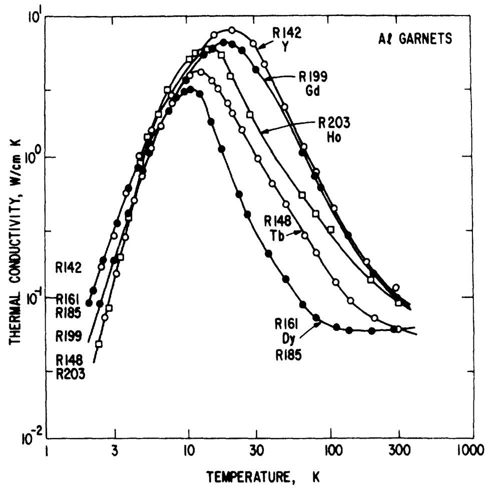

FIG. 5. Thermal conductivity vs temperature for five different rare-earth aluminum garnets. The Y and Gd exhibit no magnetic scattering; the Tb, Dy, and Ho do.

$T_N = 2.54$K. This is in contrast to some preliminary results of Landau and Dixon[8]: A number of the other paramagnetic crystals studied here are also known[68,73-76] to become antiferromagnetic at sufficiently low temperatures. The Néel temperatures are given in Table VIII. Only $Dy_3Al_5O_{12}$ has a Néel point in the temperature range that we have covered.

## V. INTERPRETATION OF RESULTS

The crystals studied here are all nonmetallic, i.e., they have no free electrons to carry the heat. Thus the heat transport is predominantly via the phonons.

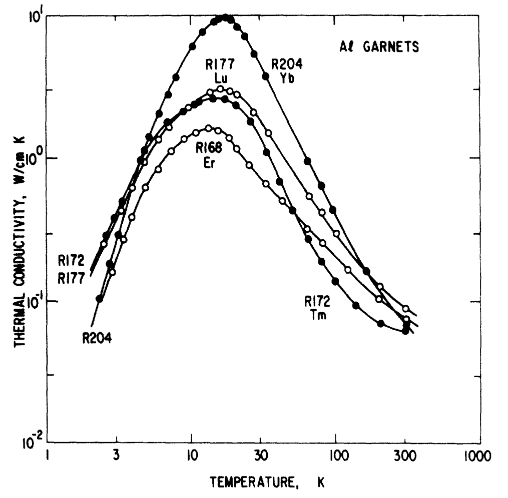

FIG. 6. Thermal conductivity vs temperature for four different rare-earth aluminum garnets. The Er and Tm exhibit magnetic scattering.

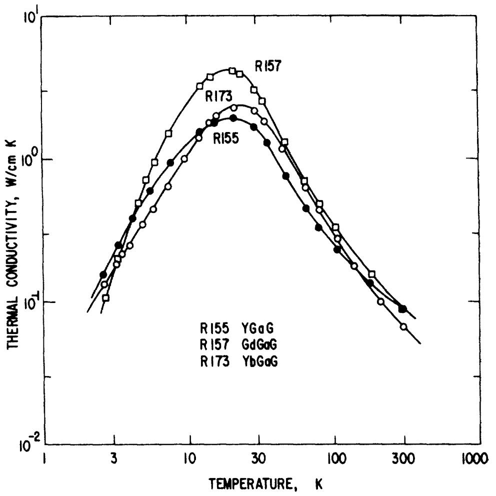

FIG. 7. Thermal conductivity vs temperature for three different rare-earth gallium garnets. There are no indications of magnetic scattering.

Only in $Dy_3Al_5O_{12}$ and $Y_3Fe_5O_{12}$ is there an ordered magnetic state between 2 and 300K. Therefore only in these two crystals is it important to consider the possibility of a magnon contribution to $\kappa$. Such a magnon contribution, if it exists, occurs[1-3,5,8] only below 20K. This means that the $\kappa$ results will be analyzed mostly in terms of phonon heat transport. For this analysis we need to consider such quantities as the Debye temperature, the average sound velocity, the lattice heat capacity, and the phonon mean free paths.

### A. Debye Temperature

In view of the rather high-impurity content of some of the crystals, some care will be necessary in analyzing these results, especially at low temperatures. However, our main concern is with two ideas. The first is to determine the $\kappa$ for the nonmagnetic crystals at temperatures near the Debye temperature $\Theta$. The second is to find out whether there is any magnetic scattering of phonons from the low-lying energy levels of the ground-state

TABLE V. Experimental thermal conductivity values for $Y_3Fe_5O_{12}$ in W/cm K.

| $T$ (K) | $Y_3Fe_5O_{12}$ $R136$ | $Ca_3Al_2Si_3O_{12}$ $R182$ |
|---|---|---|
| 30 | 1.80 | ... |
| 40 | 1.12 | 0.73 |
| 50 | 0.63 | 0.53 |
| 70 | 0.41 | 0.32 |
| 100 | 0.26 | 0.187 |
| 150 | 0.150 | 0.127 |
| 200 | 0.106 | 0.099 |
| 300 | 0.074 | 0.072 |

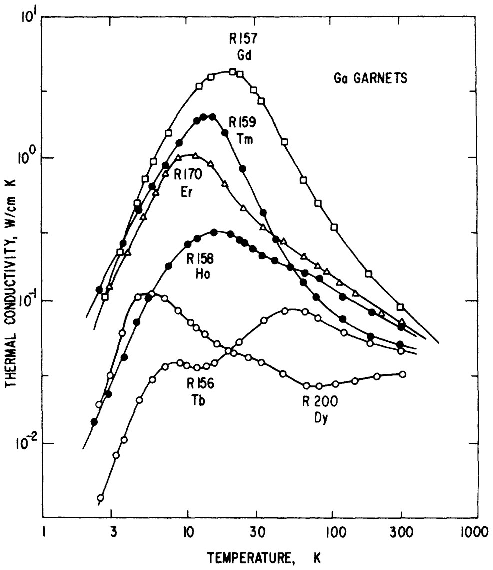

FIG. 8. Thermal conductivity vs temperature for six different rare-earth gallium garnets. All crystals other than $Gd_3Ga_5O_{12}$ exhibit magnetic scattering.

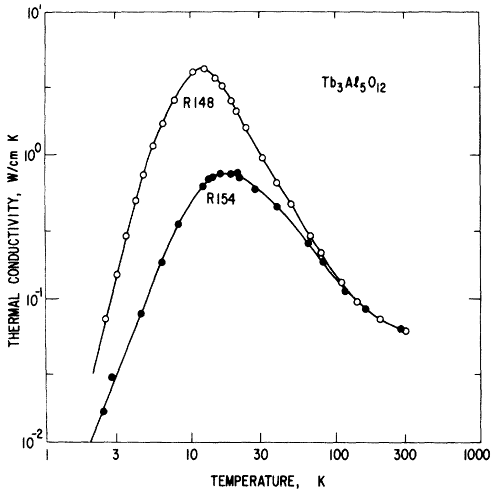

FIG. 9. Thermal conductivity vs temperature for two different crystals of $Tb_3Al_5O_{12}$. The difference is probably associated with impurities in the crystal.

multiplets of the rare-earth ions. All of these experiments have been done in zero magnetic field, so we are interested in the energy levels at zero field.

The Debye temperatures of the garnets that we have studied are, in general, not known. However, the specific heats of a few garnets have been measured, and the derived $\Theta$ values are given in Table IX. The measurements of specific-heat capacity at low temperature have been converted to Debye temperatures using the formulation of Edmonds and Petersen,[77] where

$$C_v = \tfrac{12}{5}\pi^4 k (T/\Theta)^3 / V_0 \qquad (1)$$

and $C_v$ is the specific-heat capacity per unit volume at constant volume, $k$ is Boltzmann's constant, $T$ is absolute temperature, $\Theta$ is Debye temperature, and $V_0$ is the average volume occupied by one atom of the solid. It is also possible to estimate the value of $\Theta$ from the measured elastic constants using the tables of DeLaunay.[78] For the $Y_3Fe_5O_{12}$ garnet the $\Theta = 565$ K value derived from elastic constants[79,80] is in good agreement with the value of 560 K derived from specific-heat-capacity measurements.[80,81] For all of the other garnets only one or the other type of data exists. The $\Theta$ values in Table IX derived from elastic constants[79,80,82–87] vary from 770 to 495 K, whereas those derived from the specific-heat capacity[80,81,88] vary from 715 to 460 K. Note that we have had to recompute $\Theta$ for $Nd_3Ga_5O_{12}$ and $Yb_3Ga_5O_{12}$ from the data of Onn *et al.*[88] because they did not use Eq. (1) for deriving a value of $\Theta$.

TABLE VI. Experimental thermal conductivity values for the rare-earth aluminum garnets in W/cm K.

| $T$ | Rare-earth aluminum garnet | | | | | | | | |
|---|---|---|---|---|---|---|---|---|---|
| (K) | Y<br>*R*142 | Gd<br>*R*199 | Tb<br>*R*148 | Dy<br>*R*161 | Ho<br>*R*203 | Er<br>*R*168 | Tm<br>*R*172 | Yb<br>*R*204 | Lu<br>*R*177 |
| 12 | ⋯ | ⋯ | ⋯ | 3.0 | ⋯ | ⋯ | ⋯ | ⋯ | ⋯ |
| 15 | ⋯ | ⋯ | 3.6 | 1.75 | ⋯ | 1.60 | ⋯ | ⋯ | ⋯ |
| 20 | ⋯ | ⋯ | 2.3 | 0.78 | 4.1 | 1.26 | 2.5 | 9.0 | 3.0 |
| 25 | ⋯ | 5.6 | 1.45 | 0.42 | 2.5 | 0.93 | 1.91 | 6.5 | 2.5 |
| 30 | 6.4 | 4.3 | 1.05 | 0.29 | 1.75 | 0.74 | 1.38 | 4.5 | 1.85 |
| 40 | 3.5 | 2.8 | 0.65 | 0.180 | 1.06 | 0.54 | 0.73 | 2.6 | 1.20 |
| 50 | 2.2 | 1.83 | 0.45 | 0.127 | 0.75 | 0.43 | 0.45 | 1.65 | 0.85 |
| 70 | 1.03 | 0.91 | 0.26 | 0.080 | 0.47 | 0.29 | 0.23 | 0.80 | 0.50 |
| 100 | 0.49 | 0.43 | 0.145 | 0.063 | 0.29 | 0.20 | 0.135 | 0.38 | 0.31 |
| 150 | 0.24 | 0.22 | 0.087 | 0.058 | 0.172 | 0.134 | 0.085 | 0.185 | 0.175 |
| 200 | 0.160 | 0.150 | 0.072 | 0.058 | 0.128 | 0.102 | 0.070 | 0.117 | 0.127 |
| 300 | 0.103 | 0.098 | 0.060 | 0.061 | 0.093 | 0.076 | 0.062 | 0.069 | 0.090 |

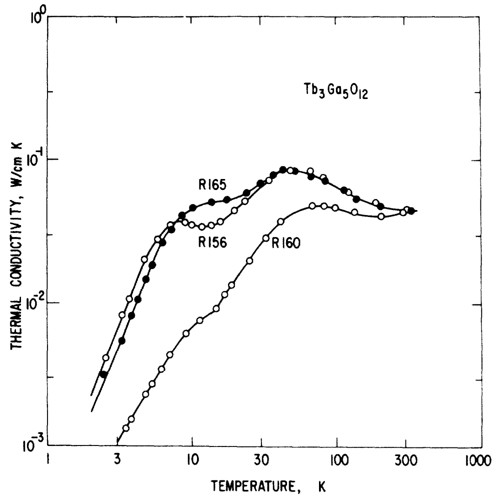

FIG. 10. Thermal conductivity vs temperature for three different crystals of $Tb_3Ga_5O_{12}$. The $\kappa$ of the melt-grown sample is lower, presumably due to an excess of Tb over the stoichiometric requirement.

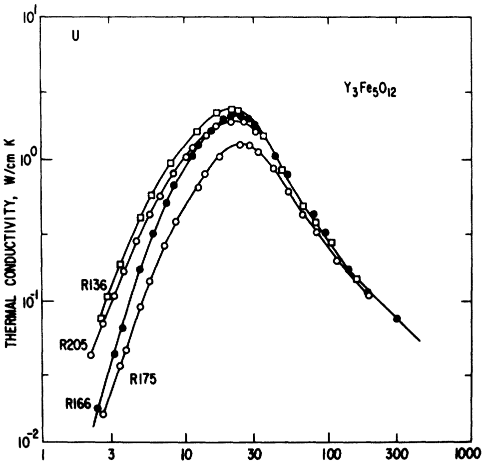

FIG. 11. Thermal conductivity vs temperature for three different crystals of $Y_3Fe_5O_{12}$. Sample $R205$ is just $R136$ reduced in diameter.

From the 14 crystals in Table IX it is possible to estimate the $\Theta$ values for other garnets by using the scaling factor derived by Steigmeier.[89] This amounts to the statement that for a series of isomorphous compounds

$$\Theta = bF, \quad F = (\bar{M} V_0)^{-1/2}, \tag{2}$$

where $b$ is some constant, $F$ is the scaling factor, $\bar{M}$ is the average atomic mass of an atom in the crystal in grams, and $V_0$ is the average volume occupied by one atom of the solid in cubic angstroms. In Fig. 13 the values of $\Theta$ from Table IX are plotted vs $F$. Four slightly different values of $b$ were chosen for the Al, Fe, Ga, and Al-Si garnets, respectively. By using Fig. 13 some of the $\Theta$ values in Table X were estimated. It is believed that these estimates are good to ± 30 K. The most serious discrepancy exists for YbGaG where the estimated $\Theta$ of 520 K disagrees with the measured value of 715 K in Table IX. It is felt that the measured value is too high, and so it was ignored.

TABLE VII. Experimental thermal conductivity values for the rare-earth gallium garnets in W/cm K.

| | Rare-earth gallium garnet | | | | | | | |
|---|---|---|---|---|---|---|---|---|
| $T$ (K) | Y $R155$ | Gd $R157$ | Tb $R156$ | Dy $R200$ | Ho $R158$ | Er $R170$ | Tm $R159$ | Yb $R173$ |
| 3 | | | 0.0064 | 0.039 | 0.024 | | | |
| 4 | | | 0.0135 | 0.083 | 0.048 | | | |
| 5 | | | 0.022 | 0.104 | 0.088 | | | |
| 7 | | | 0.035 | 0.100 | 0.155 | | | |
| 10 | | | 0.037 | 0.073 | 0.24 | | | |
| 12 | ··· | ··· | 0.034 | 0.061 | 0.27 | ··· | ··· | ··· |
| 15 | ··· | ··· | 0.036 | 0.051 | 0.30 | 0.88 | 2.0 | ··· |
| 20 | ··· | ··· | 0.045 | 0.044 | 0.29 | 0.57 | 1.25 | ··· |
| 25 | ··· | 3.7 | 0.055 | 0.040 | 0.25 | 0.43 | 0.79 | ··· |
| 30 | 1.60 | 2.9 | 0.065 | 0.036 | 0.27 | 0.35 | 0.53 | 2.0 |
| 40 | 1.04 | 1.70 | 0.080 | 0.032 | 0.190 | 0.28 | 0.29 | 1.37 |
| 50 | 0.69 | 1.12 | 0.087 | 0.029 | 0.172 | 0.24 | 0.196 | 0.95 |
| 70 | 0.39 | 0.60 | 0.082 | 0.025 | 0.150 | 0.190 | 0.120 | 0.54 |
| 100 | 0.25 | 0.35 | 0.067 | 0.025 | 0.120 | 0.148 | 0.085 | 0.30 |
| 150 | 0.160 | 0.20 | 0.055 | 0.027 | 0.092 | 0.106 | 0.063 | 0.157 |
| 200 | 0.123 | 0.140 | 0.050 | 0.029 | 0.080 | 0.085 | 0.055 | 0.105 |
| 300 | 0.090 | 0.090 | 0.045 | 0.031 | 0.065 | 0.070 | 0.049 | 0.065 |

### B. $\kappa$ near $\Theta$

Once $\Theta$ is known, then the experimental curves in Figs. 2, 3, and 5–11 can be extrapolated to give an experimental value of $\kappa$ at $T = \Theta$, i.e., $\kappa_\Theta$. These values are given in Table X. A theoretical value at $T = \Theta$ can be calculated[66] from

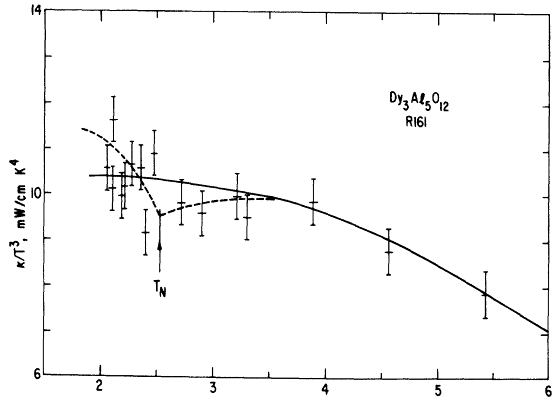

FIG. 12. Thermal conductivity divided by temperature cubed plotted vs temperature for $Dy_3Al_5O_{12}$ in the region around the Néel temperature $T_N$. The vertical bars represent the ± 5% experimental accuracy. There is no apparent anomaly in $\kappa$ at $T_N$. The dashed curve represents the greatest possible dip in $\kappa$ at $T_N$ consistent with the data, but is not a warranted interpretation of the data.

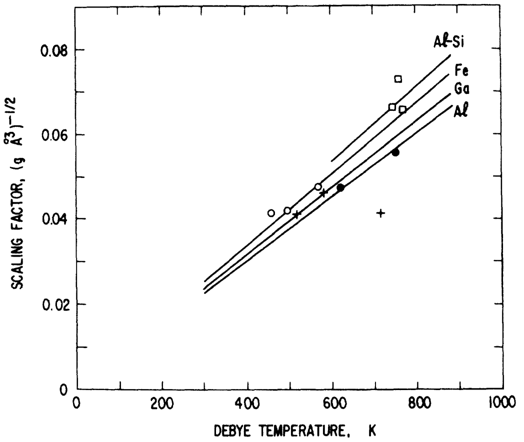

FIG. 13. Scaling factor $F$ vs Debye temperature for four different series of garnets. Each series is represented by a different type of point. The natural aluminum-silicon garnets have square points.

$$\kappa'_\Theta = 1.43\times10^{-8}\bar{M}V_0^{1/3}\Theta^2 \quad \text{W/cm K}, \qquad (3)$$

where $\bar{M}$ is given in grams, $V_0^{1/3}$ in angstroms, and $\Theta$ in deg Kelvin. The prime on $\kappa'_\Theta$ denotes a theoretical value. Values of $\kappa'_\Theta$ are given in Table X. The ratio $\kappa_\Theta/\kappa'_\Theta$ is called a crystal complexity factor (see Oliver and Slack[90]). Table X shows that this factor varies from 0.080 to 0.114 for the series of garnets, with an average value of 0.09 ± 0.01. Note that the factor for the natural garnet, grossularite, agrees with the other synthetic garnets. Also note that the ferrimagnetic garnet $Y_3Fe_5O_{12}$ agrees with the other nonmagnetic garnets. The fact that the magnetic moments on the $Fe^{3+}$ ions are ordered has not affected $\kappa_\Theta$ appreciably. The crystal complexity factor is about the same for all of the garnets, and can be considered to be a characteristic feature of the garnet lattice.

### C. Crystal-Structure Effects

The question of the effect of crystal structure on the absolute value of $\kappa$ has had a long history,[90–99] dating back to Eucken[91] in 1911. However, the theory of the effect is in a very rudimentary state. The general observation is that the larger the number of optic branches in the phonon spectrum, the lower the thermal conductivity. These considerations may become very important in garnets because there are 80 atoms in the primitive unit cell[100,101] and there are 97 optic modes[100] at the zone center. The optical-absorption[100–102] and Raman scattering[31,100,103–105] studies of garnets show that these extend at least over the phonon energy range in wave numbers of 84 to 920 cm$^{-1}$, and energies as low as 40 cm$^{-1}$ have been suggested by Koningstein[105] and 7 cm$^{-1}$ by Belyaeva *et al.*[44] Since a phonon of energy $kT$ at $T = 300$K has an energy in wave numbers of 209 cm$^{-1}$, it will be an optical phonon in $Y_3Al_5O_{12}$, and will probably have a very small or nearly zero propagation velocity. Thus we can see that such a phonon will not contribute to the thermal conduction in the crystal. This argument is similar to that used in explaining the thermal conductivity of molecular crystals.[97] This point was realized by Leibfried and Schlömann[106] in their original derivation of Eq. (3), but not was taken into account. They assumed that all of the phonons had the same propagation velocity.

We can make a crude estimate of the effect of phonons with zero group velocity on the thermal conductivity by truncating the phonon spectrum at a phonon energy less than $k\Theta$, where $\Theta$ is the Debye temperature. A somewhat similar idea was used by Holland[107] to take into account the very low group velocity of transverse acoustic phonons in Ge and Si. The value of $\kappa_D$ is determined by an integral[108] over the phonon spectrum

$$\kappa_D = \tfrac{1}{3}\int_0^{\bar{\nu}_D} \tau v^2 S\, d\bar{\nu}\ , \qquad (4)$$

where $v(\bar{\nu})$ is the group velocity of phonon of wave number $\bar{\nu}$, $\tau(\bar{\nu})$ is the lifetime of phonons of wave number $\bar{\nu}$, $S(\bar{\nu})$ is the partial contribution of phonons at $\bar{\nu}$ to the specific-heat capacity, and $\bar{\nu}_D = k\Theta/hc$ is the highest possible phonon energy in the crystal. Here $h$ is Planck's constant, $k$ is Boltzmann's constant, and $c$ is the velocity of light. The $D$ in $\kappa_D$ means all phonons up to energies of $\bar{\nu}_D$ have been included. Let us confine the problem to the temperature region $T \sim \Theta$. Then $\tau(\bar{\nu})$ is determined by phonon-phonon scattering[12,108–110] and varies as

$$\tau^{-1}(\bar{\nu}) = B\bar{\nu}^n T\ , \qquad (5)$$

where $1 \le n \le 2$, and $B$ is some constant. For $S(\bar{\nu})$, we have

$$S(\bar{\nu}) = 12\pi k\left(\frac{kT}{hv}\right)^2 \frac{x^4 e^x}{(e^x-1)^2}\ , \qquad (6)$$

where $x = hv\bar{\nu}/kT$. For $v(\bar{\nu})$ we shall assume

$$v(\bar{\nu}) = v_0 \ \text{for}\ 0 \le \bar{\nu} \le \bar{\nu}_C\ ,$$
$$v(\bar{\nu}) = 0 \ \text{for}\ \bar{\nu}_C \le \bar{\nu} \le \bar{\nu}_D\ . \qquad (7)$$

TABLE VIII. Néel temperatures of the paramagnetic rare-earth garnets.

| Crystal | $T_N$ (K) | Reference | Crystal | $T_N$ (K) | Reference |
|---|---|---|---|---|---|
| GdAlG | < 1.5 | 74 | GdGaG | < 0.35 | 74–76 |
| TbAlG | 1.35 | 74, 75 | TbGaG | < 0.6 | 74, 75 |
| DyAlG | 2.54 | 68–72 | DyGaG | < 0.36 | 68, 75, 76 |
| HoAlG | 0.85 | 74, 75 | HoGaG | < 0.35 | 74–76 |
| ErAlG | < 1.3 | 68 | ErGaG | 0.789 | 68, 75, 76 |
| TmAlG | < 1.5 | 74 | TmGaG | < 1.5 | 74 |
| YbAlG | < 1.3 | 73 | YbGaG | < 0.35 | 76 |

Here $v_0$ is some constant velocity greater than zero, and $\bar{\nu}_C$ is some critical cutoff energy in the phonon spectrum above which the phonons cannot carry any heat. If we define $K_C$ as the value of Eq. (4) when $\bar{\nu}_D$ is replaced by $\bar{\nu}_C$, we get approximately

$$\kappa_C/\kappa_D \cong (\bar{\nu}_C/\bar{\nu}_D)^{3-n} \ . \tag{8}$$

Experimentally if we use the lowest-infrared-active optic mode in $Y_3Al_5O_{12}$ at 123 $cm^{-1}$ as $\bar{\nu}_C$ and compute $\bar{\nu}_D = 521\ cm^{-1}$ from $\Theta = 750 K$, we calculate $\bar{\nu}_C/\bar{\nu}_D = 0.24$. This gives $0.056 \leq \kappa_C/\kappa_D \leq 0.24$, depending on the choice of $n$ in Eq. (5). For the garnets $\kappa_\Theta/\kappa'_\Theta = 0.09$, which is in the range of the $\kappa_C/\kappa_D$ ratio predicted by our simple model. Thus we believe that the crystal complexity factor for garnets has a reasonable explanation in terms of the phonon spectrum.

We note that the choice of $\bar{\nu}_C$ as equal in energy to the lowest-infrared-active mode of the crystal is arbitrary. The combination of infrared and Raman studies can find[100] at most 42 out of the 97 optic modes, leaving the energies of 55 modes as unknowns. We can, however, estimate the energies of the transverse and longitudinal phonons at the boundary of the Brillouin zone. This is done in the Appendix. As can be seen there, the energies of the zone-boundary acoustic phonons are comparable to that of the lowest-infrared-active mode. Hence the energy of the lowest-infrared-active mode is a good approximation to $\bar{\nu}_C$ .

TABLE IX. Values for the Debye temperatures of various garnets.

| Crystal | $\bar{M}$[a] (g) | $F$[b] | $\Theta$[c] (K) | Method[d] | Reference |
|---|---|---|---|---|---|
| Pyrope | 20.16 | 0.0726 | 760 | EC | 82 |
| Grossularite | 22.52 | 0.0654 | 770 | EC | 82 |
| Almandite | 23.8 | 0.0662 | 745 | EC | 83 |
| YAl*G* | 29.68 | 0.0558 | 750 | EC | 84, 85 |
| TbAl*G* | 40.22 | 0.0475 | 620 | EC | 86 |
| ErAl*G* | 41.43 | 0.0474 | 630 | EC | 86 |
| TmAl*G* | 41.76 | 0.0473 | 620 | EC | 86 |
| YGa*G* | 40.37 | 0.0462 | 585 | EC | 84 |
| NdGa*G* | 48.67 | 0.0411 | 715 | SH | 88 |
| GdGa*G* | 50.56 | 0.0409 | 520 | EC | 87 |
| YbGa*G* | 52.99 | 0.0408 | 715 | SH | 88 |
| YFe*G* | 36.90 | 0.0478 | 565 | EC | 79, 80 |
| YFe*G* | 36.90 | 0.0478 | 560 | SH | 80, 81 |
| EuFe*G* | 43.36 | 0.0420 | 495 | EC | 79 |
| LuFe*G* | 49.81 | 0.0416 | 460 | SH | 81 |

[a] $\bar{M}$ is the average atomic mass of an atom in the crystal.

[b] $F$ is the scaling factor [see Eq. (2)].

[c] $\Theta$ is the Debye temperature [see Eq. (1) or Ref. 78].

[d] EC means $\Theta$ was determined from the elastic constants (Ref. 78), SH means $\Theta$ was determined from the measured specific-heat capacity at liquid-helium temperatures from Eq. (1).

TABLE X. Thermal-conductivity values at the Debye temperature for crystals with no magnetic scattering.

| Crystal | $F$[a] | $\Theta$[b] (K) | $\kappa_\Theta$[c] (W/cm K) | $\kappa'_\Theta$[d] | $G$ |
|---|---|---|---|---|---|
| Grossularite | 0.0654 | 770 | 0.043 | 0.418 | 0.103 |
| YAl*G* | 0.0558 | 750 | 0.042 | 0.527 | 0.080 |
| GdAl*G* | 0.0475 | 640[e] | 0.045 | 0.521 | 0.086 |
| LuAl*G* | 0.0471 | 620[e] | 0.043 | 0.515 | 0.083 |
| YGa*G* | 0.0462 | 585 | 0.046 | 0.447 | 0.103 |
| GdGa*G* | 0.0409 | 520 | 0.051 | 0.446 | 0.114 |
| YbGa*G* | 0.0408 | 520[e] | 0.039 | 0.464 | 0.084 |
| YFe*G* | 0.0478 | 565 | 0.038 | 0.384 | 0.099 |

[a] $F$ is the scaling factor [see Eq. (2)].

[b] $\Theta$ is the Debye temperature.

[c] $\kappa_\Theta$ is the extrapolated experimental value of $\kappa$ at $T = \Theta$.

[d] $\kappa'_\Theta$ is the theoretical value of $k$ at $T = \Theta$. $\kappa_\Theta/\kappa'_\Theta$ is the crystal complexity factor $G$.

[e] Estimated $\Theta$ value (see Fig. 13).

### D. Umklapp Processes

It has long been known[111] that good crystals of $Al_2O_3$ exhibit an exponential rise in $\kappa$ with decreasing temperature that is characteristic of umklapp processes. These results on $Al_2O_3$ have been compared with a number of other crystals[12] which are isotopically pure. It is clear that the crystals have to be both chemically and isotopically pure in order to show the exponential rise in $\kappa$ at low temperatures. The one garnet studied that is almost isotopically pure is $Y_3Al_5O_{12}$. Sample *R*186 of $Y_3Al_5O_{12}$ (see Table IV) is also chemically quite pure. However, as can be seen in Fig. 3, the $\kappa$ vs $T$ curve does not rise nearly as rapidly with decreasing temperature as that[12] of $Al_2O_3$. We believe that this difference in behavior is related to the presence of the low-lying optical modes in $Y_3Al_5O_{12}$ which are not present[112,113] in $Al_2O_3$. Umklapp processes require that the sum of the wave vectors of the three interacting acoustic phonons must equal a wave vector of the reciprocal lattice. Because of the large size of the unit cell of the garnet, the wave vectors of the reciprocal lattice are very small. Hence phonons of relatively low wave vector and low energy can undergo umklapp processes in garnet. The critical phonon energy is that of the acoustic phonons at the zone boundary. Since, as is shown in the Appendix, this is of the order of $\bar{\nu}_C$, crystals of garnet behave, as far as umklapp processes are concerned, as if they have an "effective" Debye temperature comparable to $\bar{\nu}_C$; for $Y_3Al_5O_{12}$ this is 177 K. The $\kappa$ of $Y_3Al_5O_{12}$ should then have a $\kappa$ that rises with decreasing temperature as $\kappa \sim e^{+\Theta/bT}$, where $b$ is about 2 and $\Theta = 177 K$. This is in reasonable agreement with the results for $Y_3Al_5O_{12}$ in the temperature range of 30 to 70K (see Fig. 3).

The observed maximum in $\kappa$ of about 10 W/cm K at 23 K in Fig. 3 appears to be limited by the combination of this umklapp scattering with a low effective Debye temperature and the boundary scattering. Whatever impurities, dislocations, precipitates, or isotopes are present in the crystals in Fig. 3, they are, we believe, not responsible for the rather low values of $\kappa$ at the maximum.

### E. Boundary Scattering

For $T < 30\,\mathrm{K}$ the thermal conductivity in $Y_3Al_5O_{12}$ becomes dependent on the sample size, as shown in Fig. 3. At $T = 3\,\mathrm{K}$ the only scattering mechanism for phonons in pure $Y_3Al_5O_{12}$ should be boundary scattering[114] from the walls of the crystal. If this scattering is the only mechanism limiting the mean free path of the phonons, then $\kappa$ should be[114] proportional to the sample diameter. The results in Fig. 4 at 3 K show that $\kappa$ is proportional to the sample diameter $d$. The experimental relationship is

$$\kappa_B/d = 1.5(T/3\,\mathrm{K})^{2.5}\ \mathrm{W/cm^2\,K}, \tag{9}$$

where the temperature dependence comes from Fig. 3.

Theory predicts that

$$\kappa'_B/d = \tfrac{1}{3} v C_v \ , \tag{10}$$

where $v$ is some average velocity of the longitudinal and transverse phonons. We use

$$v = \tfrac{2}{3}(c_{44}/\rho)^{1/2} + \tfrac{1}{3}(c_{11}/\rho)^{1/2} \ , \tag{11}$$

where $c_{11}$ and $c_{44}$ are the elastic constants[84,85] and $\rho$ is the crystal density. The first term is for the transverse waves and the second for the longitudinal. Equation (11) is valid for the [100], [110], and [111] directions in garnet, since all of the garnets are nearly elastically isotropic, i.e., $2c_{44} = c_{11} - c_{12}$. Using this velocity and Eq. (1) for $C_v$ we get a theoretical expression for $\kappa$ in the boundary scattering region

$$\kappa'_B/d = 11.9(T/3\,\mathrm{K})^3\ \mathrm{W/cm^2\,K} \ . \tag{12}$$

This is not in very good agreement with Eq. (9). The two expressions for $\kappa_B/d$ become equal at $T = 0.05\,\mathrm{K}$.

It is not understood how the thermal conductivity at 3 K can be 8 times lower than the theoretical prediction and yet still be proportional to the sample diameter. Since all of the garnets with no magnetic scattering at 3 K, i.e., $Y_3Al_5O_{12}$, $Gd_3Al_5O_{12}$, $Yb_3Al_5O_{12}$, $Lu_3Al_5O_{12}$, $Y_3Ga_5O_{12}$, $Gd_3Ga_5O_{12}$, and $Yb_3Ga_5O_{12}$ have values of $\kappa/d$ at 3 K of $0.8 \le (K/d) \le 1.6$ W/cm² K, and even for the natural grossularite garnet $R182$, we have at 3 K a value of $\kappa/d = 0.6$ W/cm² K, we conclude that there is probably some intrinsic process in these garnets that makes the $\kappa$ in the boundary scattering region lower than that predicted by the simple theory.[114] One suggestion[115] is that perhaps only the longitudinal phonons are contributing to $\kappa$, while the transverse ones are badly scattered by interacting with the optical phonons. This makes some sense if there are optical-phonon branches at energies as low as has been suggested.[44,105] This type of scattering would keep the $d$ and $T^3$ dependence of Eq. (12) but would lower the theoretically predicted value of $\kappa$. Very pronounced effects on $\kappa$ at low temperatures of acoustic-optic-mode interaction have been seen[116] in $SrTiO_3$, for example.

At sufficiently low temperatures the thermal phonons will be lower in energy than any possible optical mode. In this limit Eq. (12) should agree with the experimental results. How low is a sufficiently low temperature? Comparison of Eqs. (9) and (12) says about 0.05 K. The present data stop at 2 K. Acoustic attenuation measurements[7,117,118] on $Y_3Ga_5O_{12}$ and $Y_3Fe_5O_{12}$ indicate that both longitudinal and transverse waves with $\bar{\nu} \le 0.3$ cm$^{-1}$ have very low attenuation in garnets at 4 K. Thus thermal phonons at ~0.1 K (where the energy of the dominant phonons is ~$4kT$ or 0.3 cm$^{-1}$) should have no bulk attenuation. Hence $\kappa$ vs $T$ measurements on $Y_3Al_5O_{12}$ from 0.1 to 2 K would help to answer the problem of whether boundary scattering agrees with the theoretical predictions.

### F. Boundary Scattering in $Y_3Fe_5O_{12}$

The $\kappa$ of sample $R136$ of $Y_3Fe_5O_{12}$ has been studied as a function of sample diameter (see Table III and Fig. 11). This sample, which has the highest $\kappa$ at 3 K of any $Y_3Fe_5O_{12}$ crystal yet studied,[1-4] has a value of $\kappa/d = 0.3$ W/cm² K at 3 K. This is substantially lower than the value found for any other garnets (see Sec. V E). Furthermore, the value of $\kappa$ at 3 K is not proportional to $d$ as $d$ is decreased. This indicates that there is some impurity scattering present in $R136$. A simple analysis of additive thermal resistivities at 3 K indicates that the boundary scattering limit of $\kappa/d$ in $R136$ would be very nearly the same as that in $Y_3Al_5O_{12}$ if the crystal were chemically pure. The presence of some kind of impurity, perhaps $Fe^{2+}$ ions produced[119] by the presence of $Si^{4+}$ ions, leads to a large residual impurity scattering in $R136$. The phonon scattering of $Fe^{2+}$ ions is known[12,120] to be large at lower temperatures. The estimated $\kappa$ of sample $R136$ as limited only by these impurities, that is, for a crystal of infinite diameter, is only 0.17 W/cm K at 3 K, i.e., only slightly larger than the value of 0.13 W/cm K measured with $d = 0.39$ cm. Since the Si concentration in $R136$ is 30 ppm, we will probably need Si concentrations of 1 ppm before the pure boundary scattering clearly dominates $\kappa$

at 3K in $Y_3Fe_5O_{12}$. Note that *R*166, which is nearly the same diameter as *R*136 but has about twice as much Si, has three times as high a thermal resistivity at 3K as *R*136. Unfortunately the impurity content of the $Y_3Fe_5O_{12}$ samples studied previously[1-5] was not measured. It may well be that the measured[1-3,5] magnetic field dependence of $\kappa$ that was interpreted as evidence of magnon heat conduction was wholly or in part caused by a magnetic field dependence of the phonon scattering from impurities. More careful work on higher-purity $Y_3Fe_5O_{12}$ needs to be done before the presence of a magnon heat transport in this crystal is fully proven.

### G. Impurity Scattering

The present studies are not very extensive with regard to the question of impurity scattering. In Sec. V F we have considered impurities in $Y_3Fe_5O_{12}$. From Table IV we see that crystals *R*186 and *R*193 of $Y_3Al_5O_{12}$ have much different impurity concentrations; however, the $\kappa$ vs *T* curves are almost identical (see Fig. 3). In fact, at the maximum in $\kappa$ at 23K the $\kappa$ of *R*193 is 20% larger than that of *R*186 in spite of its greater impurity concentration. This small difference may be attributable to the fact that *R*193 was grown at a lower temperature (~1100 °C) than was *R*186 (~2100 °C). Hence its crystal structure may be more nearly perfect. The slight variation in lattice constant in Table III may be an indication of this.

The other case where we have studied three different crystals is in $Tb_3Ga_5O_{12}$ (see Fig. 10). Here the melt-grown crystal *R*160 has a lower $\kappa$ than the other two. From Table III and Fig. 1 it can be seen that its lattice constant is also larger than for the flux-grown crystals. We believe that it contains excess Tb above the stoichiometric amount, and that this Tb occurs on the octahedral Ga sites. The crystal field on these sites is different than for the normal sites. Hence the electronic energy levels of the $^7F_6$ ground-state manifold of these $Tb^{3+}$ ions will differ from the normal ones. These give rise to new phonon scattering frequencies and hence a lower $\kappa$, in agreement with Fig. 10.

The reasons for the differences shown in Fig. 9 are unknown, but are presumably due to impurities.

### H. Phonon Scattering by Magnetic Rare-Earth Ions

So far we have investigated the phonon scattering by umklapp processes, impurities, isotopes, and sample boundaries in the nonmagnetic crystals. These same processes will also be present in all those crystals where the rare-earth ions have low-lying electronic levels. Hence, if there is any phonon scattering produced by these low-lying electronic levels, the $\kappa$ of these crystals should be reduced below that of the analogous nonmagnetic crystals. Such, indeed, can be seen to be the case in Figs. 5, 6, and 8–10. In all cases the crystals which contain ions with low-lying levels have reduced $\kappa$.

Our present hypothesis is that the dominant phonon scattering process is such that a single phonon is absorbed when a 4*f*-shell electron of a rare-earth ion makes a transition between two differnt electronic levels of its ground-state manifold. A similar phonon is later reemitted in a direction uncorrelated with that of the original one. All two- or more-phonon processes, real or virtual, are ignored. With this model we can make some further analysis of the magnetic scattering by referring to the energies given in Table I. In this resonant-scattering process the phonon being scattered must have an energy equal to the energy difference between two electronic levels of the rare-earth ion.[12] A detailed calculation for the phonon scattering form the $\bar{\nu} = 105$ cm$^{-1}$ level of $Fe^{2+}$ in MgO has recently been given.[121] The arguments for rare-earth ions will be similar. Because of the large number of low-lying levels of the rare-earth ions, many different phonon energies may be involved. However, as described in Sec. V C, phonons of energy greater than $\bar{\nu}_C$ do not contribute to the heat transport. For example, in $Dy_3Al_5O_{12}$ the infrared results show[102] $\bar{\nu}_C = 94$ cm$^{-1}$. Thus starting from the ground state of $Dy^{3+}$ in $Dy_3Al_5O_{12}$ the only possible resonance is at $\bar{\nu} = 70$ cm$^{-1}$. The strength of the phonon scattering at $\bar{\nu} = 70$ cm$^{-1}$ will depend on the electron population difference between the Kramer's doublets at 0 and 70 cm$^{-1}$. This has been calculated from Boltzmann statistics using the knowledge that all eight levels of $Dy^{3+}$ are doublets. The results are shown in Fig. 14. The next most frequent transition is that at $\bar{\nu} = 46$ cm$^{-1}$, corresponding to the $(70 \rightarrow 116)$ cm$^{-1}$ transition. This transition probability peaks at 80K as shown in Fig. 14. Other phonon scattering occurs at $\bar{\nu} = 59$ cm$^{-1}$ from the $(197 \rightarrow 256)$ cm$^{-1}$ transition, and at $\bar{\nu} = 81$ cm$^{-1}$ from the $(116 \rightarrow 197)$ cm$^{-1}$ transition (see Fig. 14). From Fig. 14 the dominant phonon scattering should occur at $\bar{\nu} = 70$ cm$^{-1}$ or 101K. A similar analysis for $Dy_3Ga_5O_{12}$, using most of the levels for $Dy^{3+}$ in $Y_3Ga_5O_{12}$ as given in Table I, exhibits phonon resonances at $\bar{\nu} = 22$, 31, 42, 47, 49, 71, and 78 cm$^{-1}$ if[102] $\bar{\nu}_C = 88$ cm$^{-1}$. In Fig. 15 we have summed the population differences for the 42, 47, and 49 cm$^{-1}$ resonances and have taken an average energy of 46 cm$^{-1}$ for the transition. Similarly, we have summed population differences for 71 and 78 cm$^{-1}$ and called the resonance energy 73 cm$^{-1}$. In making these sums we have tacitly assumed that the $\bar{\nu} = 42$, 47, and 49 cm$^{-1}$ phonon scattering cross sections are all equal. This assumption may not be justified, but will suffice at present. From Fig. 15 we see that in $Dy_3Ga_5O_{12}$, there are three important phonon resonances at $\bar{\nu} = 22$, 46, and 73

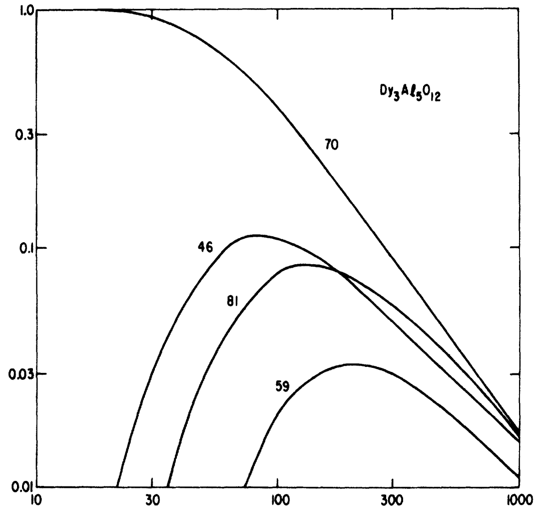

FIG. 14. Fractional population differences between the electronic levels of the *f* shell of $Dy^{3+}$ ions in $Dy_3Al_5O_{12}$. The four phonon scattering resonances are labeled according to their energies in wave numbers $cm^{-1}$.

$cm^{-1}$, or at 32, 66 and 105K.

The next step is to make an approximate computation from the experimental results of the thermal resistivity produced by the magnetic scattering. For this we simply take

$$W_{MAG}(T) = (\kappa_M)^{-1} - (\kappa_N)^{-1} , \qquad (13)$$

where $\kappa_M$ is the thermal conductivity at temperature $T$ of a crystal (say, $Dy_3Al_5O_{12}$) which posseses magnetic scattering and $\kappa_N$ is the thermal conductivity at temperature $T$ of the closest analogous crystal with no magnetic scattering (say, $Gd_3Al_5O_{12}$). The $W_{MAG}(T)$ curves for four crystals are given in Fig. 16. The vertical arrows in Fig. 16 show the dominant resonance scattering transitions to be expected for $\bar{\nu} < \bar{\nu}_C$ in the four crystals.

From Fig. 16 we see that $Dy_3Al_5O_{12}$ is probably the simplest case with the dominant scattering at only one energy of $\bar{\nu} = 70$ $cm^{-1}$. Note that $Dy_3Ga_5O_{12}$ is rather different, and has more resonances. The small changes in the crystal field in going from the aluminum to the gallium garnets make large changes in the magnetic scattering of the Dy. Both $Er_3Al_5O_{12}$ and $Tm_3Ga_5O_{12}$ also show resonance scattering, though the phonon scattering cross section of these ions is less than that of Dy. The cross section seems to be largest for Dy and decreases in the series Dy, Tb, Tm, Er, Ho, and Yb. A possible theoretical explanation of this series is not clear, but must involve the changes in wave functions of the electronic levels under strain. We also see that Kramer's ions (Dy, Er) and non-Kramer's ions (Tb, Ho, Tm) can both scatter phonons quite effectively in the 10–300K range; there is no significant difference between them as far as their effect of the thermal conductivity is concerned.

The generally observed decrease in $W_{MAG}$ in Fig. 16 for $T \gtrsim 100$K lends support to our assumption that the resonances for $\bar{\nu} > \bar{\nu}_C$ are not effective as phonon scatterers. The value of $\bar{\nu}_C$ for the four crystals in Fig. 16 is ~130K. Also, all of the possible resonances shown in Fig. 16 seem to be effective, i.e., none appear to be obviously forbidden by some selection rule. That there are some selection rules operating in certain cases for these one-phonon transitions can be seen from the $\kappa$ vs $T$ curves for $Tb_3Al_5O_{12}$ in Figs. 5 and 9. From Table I it can be seen that this crystal has a first excited state at $\bar{\nu} = 4$ $cm^{-1}$ or 5.8K. However, there is no observable effect of this transition on $\kappa$ in the 2 to 15K region. In $Tb_3Ga_5O_{12}$ there is a minimum in $\kappa$ at 12K (see Figs. 8 and 10), which indicates a level of $Tb^{3+}$ in the 2–8 $cm^{-1}$ wave-number range. The optical study on $Tb_3Ga_5O_{12}$ necessary to confirm this level has not yet been done.

The optical studies in the far infrared show[36,40] that the optical linewidths of the low-lying electronic levels of the ground-state manifold have a half-width in the vicinity of $\Delta\bar{\nu} = 5$ $cm^{-1}$. If a 5-$cm^{-1}$ wide band of phonons out of the total energy spectrum between 0 and $\bar{\nu}_C$ were being scattered, then the maximum reduction in $\kappa$ would be 5% or less. Clearly, we see reductions in $\kappa$ of factors of 10 or more. Thus we have affected phonons over a large range of energies. This may come about from the Gaussian or Lorentzian tails of the single scattering resonance,[14] from the effects of normal

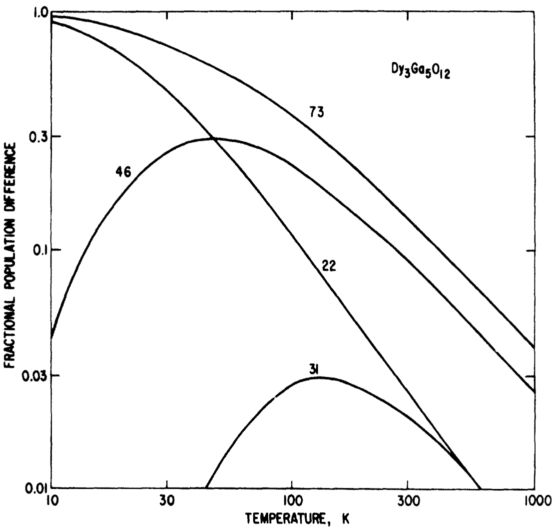

FIG. 15. Fractional population differences between the electronic levels of the *f* shell of $Dy^{3+}$ ions in $Dy_3Ga_5O_{12}$. The four phonon scattering resonances are labeled according to their energies in wave numbers $cm^{-1}$.

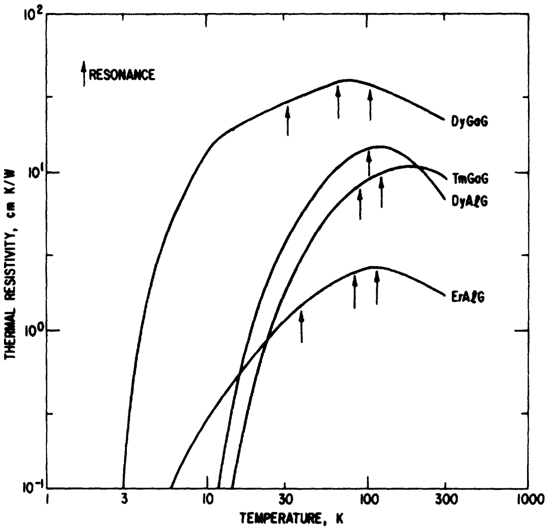

FIG. 16. Thermal resistivity vs temperature of four different garnets. The possible phonon scattering resonances are indicated by vertical arrows.

processes[108,109] in the phonon-phonon interactions, from neglected Raman processes, or some other mechanism. Detailed calculations and perhaps further experiments are needed to clarify this problem.

### J. Cooperative Effects

If a crystal is in an ordered magnetic state, then quantum excitations of the magnetic lattice, i.e., magnons, can transport thermal energy. The real question about such a magnon thermal conductivity is whether the mean free path of the magnons is sufficiently large to provide a measureable contribution to $\kappa$. From Table VIII we see that $Dy_3Al_5O_{12}$ is the only rare-earth garnet with a Néel temperature high enough to be studied with the present apparatus. The lower-temperature limit of the data is 2 K. The results for $Dy_3Al_5O_{12}$ are given in Fig. 5. In Fig. 5 we see that $\kappa$ varies about as $T^3$ below 4 K. In Fig. 12 we have plotted $\kappa/T^3$ for all 16 of the data points in the 2–6 K range. The vertical bars represent the ± 5% accuracy of the measurements. The solid curve in Fig. 12 is a good fit to these data, and shows no anomaly in $\kappa$ through the Néel point $T_N$. Landau and Dixon[8] report a minimum in $\kappa$ at $T_N$. The dashed curve in Fig. 12 shows the largest anomaly that might be constructed from the present data. We do not think that the data really warrant such an interpretation. We conclude that if there is a magnon contribution to $\kappa$ near $T_N$, it is less than 10% of the lattice $\kappa$, and may be zero. Landau and Dixon[8] do not state how large their magnon contribution to $\kappa$ is in the 2–2.5 K range.

The possible cooperative effects in $Y_3Fe_5O_{12}$ have already been considered in Sec. V F.

## VI. OTHER RARE-EARTH GARNETS

We have not measured the $\kappa$ of any garnets of the rare-earth ions $Ce^{3+}$, $Pr^{3+}$, $Nd^{3+}$, $Sm^{3+}$, or $Eu^{3+}$. The low-lying electronic levels of these ions are given in Table XI based on data[23–26,32,39,122–125] from the literature. It is known[126,127] that Ce does not form either Al or Ga garnets, whereas Pr, Nd, Sm, and Eu form Ga but not Al garnets. If we consider only the possible resonance transitions for phonons of energy less than $\bar{\nu}_C$ which is about[101] 90 $cm^{-1}$ for the gallium garnets, then from Table XI we conclude that $Pr_3Ga_5O_{12}$ should show pronounced magnetic scattering effects from 20 to 100 K and that $Nd_3Ga_5O_{12}$ may show some at about 100 K. The $Sm_3Ga_5O_{12}$ and $Eu_3Ga_5O_{12}$ garnets should show little if any magnetic scattering.

TABLE XI. Energy levels of the low-lying multiplets of trivalent rare-earth ions in garnets.

| Ion | Host crystal | Multiplet | Number of levels | Wave numbers of observed levels ($cm^{-1}$) | Reference |
|---|---|---|---|---|---|
| $Ce^{3+}$ | YGaG | ${}^2F_{5/2}$ | 3 | 0, 139, 402 | 122 |
| $Pr^{3+}$ | YAlG | ${}^3H_4$ | 9 | 0, 19, 50, 573, others >600 | 123 |
| $Pr^{3+}$ | YGaG | ${}^3H_4$ | 9 | 0, 23, 39, 538, others >600 | 123 |
| $Nd^{3+}$ | YAlG | ${}^4I_{9/2}$ | 5 | 0, 133, 201, 307, 857 | 23–25 |
| $Nd^{3+}$ | YGaG | ${}^4I_{9/2}$ | 5 | 0, 80, 174, 240 | 26 |
| $Sm^{3+}$ | YAlG | ${}^6H_{5/2}$ | 3 | 0, 142, 251 | 124 |
| $Sm^{3+}$ | YGaG | ${}^6H_{5/2}$ | 3 | 0, 47, 136 | 124 |
| $Sm^{3+}$ | SmGaG | ${}^6H_{5/2}$ | 3 | 0, 90, 190 | 39 |
| $Eu^{3+}$ | YAlG | ${}^7F_0$ | 1 | 0 | 32 |
| $Eu^{3+}$ | YAlG | ${}^7F_1$ | 3 | 286, 307, 455 | 32 |
| $Eu^{3+}$ | YGaG | ${}^7F_0$ | 1 | 0 | 125 |
| $Eu^{3+}$ | YGaG | ${}^7F_1$ | 3 | 307, 345, 388 | 125 |

If the scattering cross section is large enough, it might also be possible to see a magnetic scattering effect from $Pr^{3+}$ impurities in $Y_3Al_5O_{12}$ crystals or $Sm^{3+}$ in $Y_3Ga_5O_{12}$ if the impurity-ion-to-Y ratio is made as high[128] as 0.01–0.05. Similarly, $Tb^{3+}$, $Dy^{3+}$, $Ho^{3+}$, and $Tm^{3+}$ impurities in $Y_3Al_5O_{12}$ or $Y_3Ga_5O_{12}$ should show the same effects. The previous experiments[4] on the $\kappa$ of $Nd^{3+}$-doped $Y_3Al_5O_{12}$ showed no resonance-scattering–type dips in the $\kappa$ vs $T$ curves. The reason seems to be that $Nd^{3+}$ in $Y_3Al_5O_{12}$ has no possible resonance transitions starting from the ground state at energies less than $\bar{\nu}_C$ (see Table XI). The major effect[4] of Nd on the $\kappa$ of $Y_3Al_5O_{12}$ is probably due to mass-difference scattering since Nd has a considerably larger atomic mass than Y. A similar situation appears to apply to the $\kappa$ measurements[19] on $Nd^{3+}$-doped $CaWO_4$. The electronic levels[129] of $Nd^{3+}$ in $CaWO_4$ all lie above $\bar{\nu}_C = 86$ cm$^{-1}$, as determined[130] from infrared and Raman data.

## VII. CONCLUSIONS

The study of the thermal conductivity of the rare-earth aluminum and gallium garnets has shown that in the nonmagnetic garnets the heat is carried by phonons of energies from zero to some cutoff energy $\bar{\nu}_C$. The value of $\bar{\nu}_C$ is approximately that of the lowest optical-phonon branch of the crystal, and is much lower than the phonon energy corresponding to the Debye temperature, $\bar{\nu}_D$. This feature accounts for the low thermal conductivity of all nonmagnetic crystals of the garnet structure for $T \gtrsim 30$K. These crystals also have unusually low thermal conductivities in the boundary-scattering region where $T < 10$K. The explanation of this behavior is not understood.

The magnetic garnets, i.e., those in which the rare-earth ions have partially filled $4f$ shells, can be divided into two groups. In the first group are the garnets of Gd and Yb where the lowest-lying electronic level of the rare-earth ion lies at an energy much greater than $\bar{\nu}_C$ above the ground state. The thermal conductivity of these garnets is almost identical to that of the nonmagnetic garnets. In the second group of magnetic garnets, i.e., those of Tb, Dy, Ho, Er, and Tm, there are electronic levels of the ground-state manifold that have energies less than $\bar{\nu}_C$. In these garnets the thermal conductivity is further suppressed by a magnetic scattering which seems to be dominated by a one-phonon resonance scattering process for those phonons whose energies are equal to the energy difference between two electronic levels. The effectiveness of this magnetic scattering is largest for Dy and decreases in the series Dy, Tb, Tm, Er, and Ho. Its temperature dependence is closely related to the thermally determined population differences between the two levels involved in the transition.

The natural garnet $Ca_3Al_2Si_3O_{12}$ and the synthetic $Y_3Fe_5O_{12}$ behave essentially like the nonmagnetic garnets. Impurities of $Fe^{2+}$ in both $Y_3Fe_5O_{12}$ and in other natural garnets such as $Mg_3Al_2Si_3O_{12}$ appear to be responsible for some phonon scattering that reduces the thermal conductivity.

## ACKNOWLEDGMENTS

The authors wish to thank J. H. McTaggart and G. Brower for their help in growing several of the crystals and in measuring the thermal conductivity. They also wish to thank Dr. W. P. Wolf and Dr. C. B. Rubinstein for supplying various garnet crystals used in this study.

## APPENDIX

The values of the transverse acoustic or TA and the longitudinal acoustic or LA phonon energies at the Brillouin-zone boundary in the [100] direction can be estimated for $Y_3Al_5O_{12}$. From the elastic constants[84,85] we can calculate the sound velocities as

$$v_L = (c_{11}/\rho)^{1/2} = 8.59 \times 10^5 \text{ cm/sec},$$

$$v_T = (c_{44}/\rho)^{1/2} = 5.03 \times 10^5 \text{ cm/sec}.$$

We now assume the simplest dispersion curve possible[131] for the acoustic branches, i.e.,

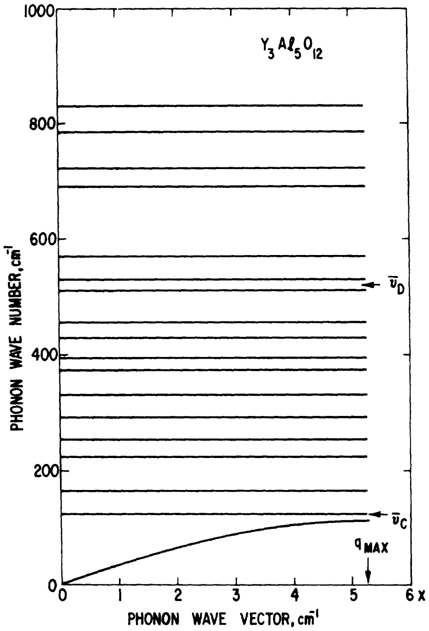

FIG. 17. Schematic of the phonon energy in wave numbers vs phonon momentum in the [100] direction in $Y_3Al_5O_{12}$. The only optic branches shown are those that are infrared active. The TA and LA branches are averaged into a single acoustic branch.

$$\bar{\nu} = \bar{\nu}_{\max} \sin \tfrac{1}{4} q a_0 \ , \tag{A1}$$

where $\bar{\nu}$ is the phonon energy in wave numbers, $q$ is the phonon wave vector ($= 2\pi/\lambda$), $\lambda$ is the phonon wavelength, $a_0$ is the lattice constant of the crystal, $\bar{\nu}_{\max}$ is the phonon energy at the zone boundary in the [100] direction. Note $q_{\max} = 2\pi/a_0$ in this bcc crystal. The phase velocity of a phonon is just

$$v = 2\pi c \frac{d\bar{\nu}}{dq} \ , \tag{A2}$$

where $c$ is the velocity of light in free space. So we get

$$v = \tfrac{1}{2}(\pi a_0 c \bar{\nu}_{\max}) \cos \tfrac{1}{4} q a_0 \ . \tag{A3}$$

Near $q = 0$ we have $v$ equal to the sound velocity. Thus we can get $\bar{\nu}_{\max}$ for transverse waves in terms of the sound velocity $v_T$ as

$$\bar{\nu}_{\max T} = 2v_T/\pi a_0 c \tag{A4}$$

and similarly for $\bar{\nu}_{\max L}$. The result for $Y_3Al_5O_{12}$ in the [100] direction at the zone boundary is

$$\bar{\nu}_{\max T} = 152\ \text{cm}^{-1}, \quad \bar{\nu}_{\max L} = 89\ \text{cm}^{-1} \ .$$

An average value for acoustic phonons is

$$\bar{\nu}_{\max} = \tfrac{1}{3}(2\bar{\nu}_{\max T} + \bar{\nu}_{\max L}) = 110\ \text{cm}^{-1} \ . \tag{A5}$$

This value is close to the lowest-infrared-active mode at $\bar{\nu} = 123\ \text{cm}^{-1}$. Hence we choose this latter value as a convenient cutoff energy (see Fig. 17 for a plot of the acoustic and optic[60] phonons).

Since the garnets are close to being elastically isotropic, the $\bar{\nu}_C$ values are almost the same for all propagation directions in the crystal. Hence our results for the [100] direction are generally valid.

---

[*] Work supported in part by U. S. Air Force Materials Laboratory, under Contract No. F33615-69-C-1286.

[1] B. Lüthi, J. Phys. Chem. Solids 23, 35 (1962).

[2] S. A. Friedberg and E. D. Harris, in *Proceedings of the Eighth International Conference on Low Temperature Physics* (Butterworths, London, 1963), p. 302.

[3] R. L. Douglass, Phys. Rev. 129, 1132 (1963).

[4] D. W. Oliver and G. A. Slack, J. Appl. Phys. 37, 1542 (1966).

[5] J. E. Rives, G. S. Dixon, and D. Walton, J. Appl. Phys. 40, 1555 (1969); J. E. Rives, Q. Khalid, and D. Walton, Bull. Am. Phys. Soc. 15, 1314 (1970).

[6] P. H. Klein and W. J. Croft, J. Appl. Phys. 38, 1603 (1967).

[7] M. G. Holland, IEEE Trans. Sonics and Ultrasonics SU15, 18 (1968).

[8] D. P. Landau and G. S. Dixon, Bull. Am. Phys. Soc. 15, 1381 (1970).

[9] C. M. Bhandari and G. S. Verma, Phys. Rev. 152, 731 (1966).

[10] A. W. Joshi and K. P. Sinha, Proc. Phys. Soc. (London) 88, 685 (1966).

[11] E. D. Devyatkova and V. V. Tikhonov, Fiz. Tverd. Tela 9, 772 (1967) [Sov. Phys. Solid State 9, 604 (1967)].

[12] G. A. Slack and S. Galginaitis, Phys. Rev. 133, A253 (1964).

[13] G. A. Slack, in *Proceedings of the Fourth Conference on Thermal Conductivity* (U. S. Naval Radiological Defense Laboratory, San Francisco, 1964), paper 1-C.

[14] G. A. Slack, S. Roberts, and J. T. Vallin, Phys. Rev. 187, 511 (1970).

[15] I. P. Morton and H. M. Rosenberg, Phys. Rev. Letters 8, 200 (1962).

[16] P. V. E. McClintock, I. P. Morton, R. Orbach, and H. M. Rosenberg, Proc. Roy. Soc. (London) A298, 359 (1967).

[17] G. T. Fox, M. W. Wolfmeyer, J. R. Dillinger, and D. L. Huber, Phys. Rev. 181, 1308 (1969).

[18] D. Walton, Phys. Rev. B 1, 1234 (1970).

[19] M. G. Holland, J. Appl. Phys. 33, 2910 (1962).

[20] E. D. Devyatkova, V. P. Zhuze, A. V. Golubkov, V. M. Sergeeva, and I. A. Smirnov, Fiz. Tverd. Tela 6, 430 (1964) [Sov. Phys. Solid State 6, 343 (1964)].

[21] J. Loriers, J. Suchet, G. Weill, and G. Collin, Compt. Rend. 261, 2219 (1965).

[22] V. P. Zhuze, V. I. Novikov, V. M. Sergeeva, and S. S. Shalyt, Fiz. Tverd. Tela 11, 2192 (1969) [Sov. Phys. Solid State 11, 1750 (1970)].

[23] J. A. Koningstein and J. E. Geusic, Phys. Rev. 136, A711 (1964).

[24] P. P. Feofilov, V. A. Timofeeva, M. N. Tolstoi, and L. M. Belyaev, Opt. i Spektroskopiya 19, 817 (1965) [Opt. Spectry. (USSR) 19, 451 (1965)].

[25] A. A. Kaminskii, Zh. Eksperim. i Teor. Fiz. 51, 49 (1966) [Sov. Phys. JETP 24, 33 (1967)].

[26] J. A. Koningstein, J. Chem. Phys. 44, 3957 (1966).

[27] G. H. Dieke and H. M. Crosswhite, Appl. Opt. 2, 675 (1963).

[28] A. H. Cooke, T. L. Thorp, and M. R. Wells, Proc. Phys. Soc. (London) 92, 400 (1967).

[29] J. A. Koningstein, Chem. Phys. Letters 2, 213 (1968).

[30] J. A. Koningstein and G. Schaack, Phys. Rev. B 2, 1242 (1970).

[31] J. A. Koningstein and G. Schaack, J. Opt. Soc. Am. 60, 755 (1970).

[32] J. A. Koningstein, Phys. Rev. 136A, 717 (1964).

[33] T. D. Knight and D. L. Huber, J. Appl. Phys. 39, 1069 (1968).

[34] K. A. Gehring, M. J. M. Leask, and J. H. M. Thornley, J. Phys. C 2, 484 (1969).

[35] J. A. Koningstein and T. Ng, Solid State Commun. 7, 351 (1969).

[36] J. Blanc, D. Brochier, and A. Ribeyron, Phys. Letters 33A, 201 (1970).

[37] P. Grünberg, K. H. Hellwege, and S. Hüfner, Physik Kondensierten Materie 6, 95 (1967).

[38] P. Grünberg, S. Hüfner, E. Orlich, and J. Schmitt, Phys. Rev. 184, 285 (1969).

[39] M. Veyssie and B. Dreyfus, J. Phys. Chem. Solids 28, 499 (1967).

[40] R. C. Milward, Phys. Letters A25, 19 (1967).

[41] L. F. Johnson, J. E. Geusic, and L. G. Van Uitert, Appl. Phys. Letters 8, 200 (1966).

[42] A. J. Sievers and M. Tinkham, Phys. Rev. 129, 1995 (1963).

[43] D. G. Onn, H. Meyer, and J. P. Remeika, Phys. Rev. 156, 663 (1967).

[44] A. I. Belyaeva, V. N. Pavlov, and A. V. Antonov, Opt. i Spectroskopiya 27, 287 (1969) [Opt. Spectry. (USSR) 27, 151 (1969)].

[45] L. F. Johnson, J. F. Dillon, and J. P. Remeika, J. Appl. Phys. 40, 1499 (1969).

[46] L. F. Johnson, J. F. Dillon, and J. P. Remeika, Phys. Rev. B 1, 1935 (1970).

[47] H. Kamimura and T. Yamaguchi, Phys. Rev. B 1, 2902 (1970).

[48] K. G. Hellwege, S. Hüfner, M. Schinkman, and H. Schmidt, Physik Kondensierten Materie 4, 397 (1966).

[49] B. Dreyfus, J. Verdone, and M. Veyssie, J. Phys. Chem. Solids 26, 107 (1965).

[50] H. M. Crosswhite and H. W. Moos, *Optical Properties of Ions in Crystals* (Interscience, New York, 1967), p. 7.

[51] R. W. Bierig and L. Rimai, J. Appl. Phys. 36, 1199 (1965).

[52] L. F. Johnson, J. E. Geusic, and L. G. Van Uitert, Appl. Phys. Letters 7, 127 (1965).

[53] J. A. Koningstein, Theoret. Chim. Acta 5, 327 (1966).

[54] J. J. Pearson, G. F. Herrmann, and R. A. Buchanan, J. Appl. Phys. 39, 980 (1968).

[55] R. A. Buchanan, J. J. Pearson, and G. F. Herrmann, Solid State Commun. 7, 195 (1969).

[56] R. A. Buchanan, K. A. Wickersheim, J. J. Pearson, and G. F. Herrmann, Phys. Rev. 159, 245 (1967).

[57] G. A. Slack and R. M. Chrenko, J. Opt. Soc. Am. (to be published).

[58] Rare-Earth Division, American Potash and Chemical Corp., West Chicago, Ill.

[59] Crystal Products Department, Electronics Division, Union Carbide Corp., Boston, Mass.

[60] G. A. Slack, D. W. Oliver, R. M. Chrenko, and S. Roberts, Phys. Rev. 177, 1308 (1969).

[61] F. Bertaut and F. Forrat, Compt. Rend. 244, 96 (1957).

[62] F. Euler and J. A. Bruce, Acta Cryst. 19, 971 (1965).

[63] C. B. Rubenstein and R. L. Barns, Am. Mineral. 50, 782 (1965).

[64] S. J. Schneider, R. S. Roth, and J. L. Waring, J. Res. Natl. Bur. Std. 65A, 345 (1961).

[65] G. A. Slack, Phys. Rev. 122, 1451 (1961).

[66] G. A. Slack, Phys. Rev. 126, 427 (1962).

[67] G. A. Slack, J. Appl. Phys. 35, 3460 (1964).

[68] M. Ball, G. Garton, M. J. M. Leask, D. Ryan, and W. P. Wolf, J. Appl. Phys. 32S, 267 (1961).

[69] M. Ball, M. J. M. Leask, W. P. Wolf, and A. F. G. Wyatt, J. Appl. Phys. 34, 1104 (1963).

[70] B. E. Keen, D. P. Landau, B. Schneider, and W. P. Wolf, J. Appl. Phys. 37, 1120 (1966).

[71] B. E. Keen, D. P. Landau, and W. P. Wolf, J. Appl. Phys. 38, 967 (1967).

[72] A. Herpin and P. Meriel, Compt. Rend. 259, 2416 (1964).

[73] M. Ball, G. Garton, M. J. M. Leask, and W. P. Wolf, in *Proceedings of the Seventh International Conference on Low Temperature Physics*, 1960 (University of Toronto Press, Toronto, Canada, 1961), p. 128.

[74] W. P. Wolf, M. Ball, M. T. Hutchings, M. J. M. Leask, and A. F. G. Wyatt, J. Phys. Soc. Japan Suppl. B1, 17, 443 (1962).

[75] A. H. Cooke, T. L. Thorp, and M. R. Wells, Proc. Phys. Soc. (London) 92, 400 (1967).

[76] D. G. Onn, H. Meyer, and J. P. Remeika, Phys. Rev. 156, 663 (1967).

[77] D. T. Edmonds and R. G. Peterson, Phys. Rev. Letters 2, 499 (1959).

[78] J. DeLaunay, J. Chem. Phys. 22, 1676 (1954); 24, 1071 (1956); 30, 91 (1959).

[79] T. B. Bateman, J. Appl. Phys. 37, 2194 (1966).

[80] S. S. Shinozaki, Phys. Rev. 122, 388 (1961).

[81] A. B. Harris and H. Meyer, Phys. Rev. 127, 101 (1962).

[82] T. V. Ryzhova, L. M. Reshchikova, and K. S. Aleksandrov, Izv. Akad. Nauk SSSR, Fiz. Zemli No. 7, 52 (1966) [Izv. Solid Earth Phys. No. 7, 447 (1966)].

[83] N. Soga, J. Geophys. Res. 72, 4227 (1967).

[84] E. G. Spencer, R. T. Denton, T. B. Bateman, W. B. Snow, and L. G. Van Uitert, J. Appl. Phys. 34, 3059 (1963).

[85] W. J. Alton and A. J. Barlow, J. Appl. Phys. 38, 3023 (1967).

[86] J. D. Young (unpublished).

[87] L. J. Graham and R. Chang, J. Appl. Phys. 41, 2247 (1970).

[88] D. G. Onn, H. Meyer, and J. P. Remeika, Phys. Rev. 156, 663 (1967).

[89] E. F. Steigmeier, Appl. Phys. Letters 3, 6 (1963).

[90] D. W. Oliver and G. A. Slack, J. Appl. Phys. 37, 1542 (1966).

[91] A. Eucken, Ann. Physik 34, 185 (1911).

[92] A. Eucken, in *Quanten-Theorie und Chemie*, edited by H. Falkenhagen (Hirzel, Leipzig, 1928), p. 112.

[93] A. Eucken and E. Kuhn, Z. Physik Chem. (Frankfurt) 134, 193 (1928).

[94] M. Blackman, Phil. Mag. 19, 989 (1935).

[95] W. A. Wooster, Z. Krist. 95, 138 (1936).

[96] R. W. Keyes, Phys. Rev. 115, 564 (1959).

[97] G. A. Slack, Phys. Rev. 139, A507 (1965).

[98] A. Missenard, *Conductive Thermique des Solides, Liquides, Gaz et de Leurs Mélanges* (Eyrolles, Paris, 1965), Chap. II.

[99] D. P. Spitzer, J. Phys. Chem. Solids 31, 19 (1970).

[100] J. P. Hurrell, S. P. S. Porto, I. F. Chang, S. S. Mitra, and R. P. Bauman, Phys. Rev. 173, 851 (1968).

[101] G. A. Slack, D. W. Oliver, R. M. Chrenko, and S. Roberts, Phys. Rev. 177, 1308 (1969).

[102] N. T. McDevitt, J. Opt. Soc. Am. 59, 1240 (1969).

[103] J. A. Koningstein and O. S. Mortensen, J. Mol. Spectry. 27, 343 (1968).

[104] J. A. Koningstein and T. Ng, J. Opt. Soc. Am. 58, 1462 (1968).

[105] J. A. Koningstein, Chem. Phys. Letters 3, 303 (1969).

[106] G. Leibfried and E. Schlömann, Nachr. Akad. Wiss. Göttingen, II. Math. Physik. Kl. 4, 71 (1954).

[107] M. G. Holland, Phys. Rev. 132, 2461 (1963).

[108] P. G. Klemens, in *Solid State Physics*, edited by F. Seitz and D. Turnbull (Academic, New York, 1958), Vol. 7, p. 1; also pp. 40 and 46.

[109] P. G. Klemens, in *Thermal Conductivity*, edited by R. P. Tye, (Academic, New York, 1969), Vol. 1, p. 1; also p. 49.

[110] V. Ambegaokar, Phys. Rev. 114, 488 (1959).

[111] R. Berman, F. E. Simon, and J. Wilks, Nature 168, 277 (1951).

[112] A. S. Barker, Phys. Rev. 132, 1474 (1963).

[113] S. P. S. Porto and R. S. Krishnan, J. Chem. Phys. 47, 1009 (1967).

[114] P. D. Thacher, Phys. Rev. 156, 975 (1967).

[115] P. G. Klemens (private communication).

[116] E. F. Steigmeier, Phys. Rev. 168, 523 (1968).

[117] M. G. Holland, A. E. Paladino, and R. W. Bierig, J. Appl. Phys. 38, 4100 (1967).

[118] M. F. Lewis and E. Patterson, J. Appl. Phys. 39, 1932 (1968).

[119] D. L. Wood and J. P. Remeika, J. Appl. Phys. 37, 1232 (1966).

[120] G. T. Fox, M. W. Wolfmeyer, J. R. Dillinger, and D. L. Huber, Phys. Rev. 165, 898 (1968).

[121] I. P. Morton and M. F. Lewis, Phys. Rev. B 3, 552 (1971).

[122] G. F. Herrmann, J. J. Pearson, K. A. Wickersheim, and R. A. Buchanan, J. Appl. Phys. 37, 1312 (1966).

[123] F. N. Hooge, J. Chem. Phys. 45, 4504 (1966).

[124] P. Grünberg, Z. Physik 225, 376 (1969).

[125] J. A. Koningstein, J. Chem. Phys. 42, 3195 (1965).

[126] F. Bertaut and F. Forrat, Compt. Rend. 243, 1219 (1956).

[127] H. Brusset, H. Gillier-Pandraud, and J. L. Berdot, Bull. Soc. Chim. (France) 1206 (1967).

[128] M. Kestigian and W. W. Holloway, Jr., J. Crystal Growth 3-4, 455 (1968).

[129] D. Sengupta and J. O. Artman, J. Chem. Phys. 50, 5308 (1969).

[130] R. K. Khanna and E. R. Lippincott, Spectrochim. Acta 24A, 905 (1968).

[131] L. Brillouin, *Wave Propagation in Periodic Structures* (McGraw-Hill, New York, 1946), Chap. III.

---

PHYSICAL REVIEW B VOLUME 4, NUMBER 2 15 JULY 1971

# Self-Consistent Local Orbitals for NaCl, NaBr, KCl, and KI[†]

**A. Barry Kunz**
*Department of Physics and Materials Research Laboratory.*
*University of Illinois, Urbana, Illinois* 61801

(Received 25 February 1971)

Using the Adams-Gilbert local-orbitals theory, accurate to first order in interatomic overlap, it has been possible to obtain self-consistent local orbitals for several fcc alkali halide crystals. In this paper, results are reported for NaCl, NaBr, KCl, and KI. In this calculation, nearest neighbors are considered exactly while more distant neighbors are considered in a point-ion model. The method of Roothaan is used to obtain the results. All relativistic effects are neglected in this calculation.

## I. INTRODUCTION

Since the introduction of exact localized-orbitals theories by Adams[1] and Gilbert,[2] one has been given a method capable of treating the exact self-consistent Hartree-Fock problem for certain extended systems. The Adams-Gilbert equation is in general rather cumbersome and it is useful to simplify the equation. A pseudopotential method of obtaining such a simple local-orbitals equation has been proposed by Anderson.[3] The author has suggested that one can simplify the Adams-Gilbert equation by expanding it in powers of interatomic overlap, and retaining terms to first order.[4] This seems justified for such systems as the alkali halides where the interatomic overlaps are typically of the order 0.1 or less.[5] Previously we have reported such solutions for the Li$X$ crystals.[6] Here, as previously, we adopt the analytic Hartree-Fock technique of Roothaan[7] in a somewhat modified form. In this present work, the calculations for NaCl and NaBr were performed using the same computer code as were used in the work for the lithium halide crystals. In the case of KCl and KI, a modified version of our previous code was used. The chief effect of the modified code is to produce single-particle energies with the error in the fifth or sixth significant figure rather than in the fourth figure as was the case of the lithium halide crystals. Differences of this sort are not significant for most solid-state problems.

The local orbitals, which the author and others previously obtained for the Li$X$ crystals, and also the current results for NaCl and NaBr have proven useful for band-structure calculations.[8] Calculations of elastic constants, using these local orbitals, seem to improve the agreement between theory and experiment with respect to computing the deviation from the Cauchy relations for the lithium halides.[9]

The general results of band calculations using Hartree-Fock theory and self-consistent local orbitals are in general in poor agreement with previous results for these materials.[8,10] This is especially true for the Slater type of exchange or modification of it. In general, the Hartree-Fock results have valence bands which are substantially broader than previous calculations led one to expect.

The computer codes used in this study were developed by the author for the IBM 360-75 computer at the University of Illinois. In Sec. II, we provide a brief description of the local-orbitals technique and our numerical methods. In Sec. III, numerical results are presented for NaCl, NaBr,